

**SURFACE-ENHANCED RAMAN SCATTERING USING
FLUORESCENCE-QUENCHED CARBON QUANTUM
DOTS FOR MERCURY ION DETECTION**

Miss Andaru Dena Prasiwi



**A Thesis Submitted in Partial Fulfillment of the Requirements
for the Degree of Master of Science in Chemistry
Department of Chemistry
FACULTY OF SCIENCE
Chulalongkorn University
Academic Year 2020
Copyright of Chulalongkorn University**

เซอร์เฟซเอนฮานซ์รามานสแกตเตอริงโดยใช้คาร์บอนควอนตัมดอตซึ่งถูกดัดแปลงออกเรสเซนซ์เพื่อ
การตรวจวัดไอออนปรอท



วิทยานิพนธ์นี้เป็นส่วนหนึ่งของการศึกษาตามหลักสูตรปริญญาวิทยาศาสตรมหาบัณฑิต
สาขาวิชาเคมี ภาควิชาเคมี
คณะวิทยาศาสตร์ จุฬาลงกรณ์มหาวิทยาลัย
ปีการศึกษา 2563
ลิขสิทธิ์ของจุฬาลงกรณ์มหาวิทยาลัย

Thesis Title	SURFACE-ENHANCED RAMAN SCATTERING USING FLUORESCENCE-QUENCHED CARBON QUANTUM DOTS FOR MERCURY ION DETECTION
By	Miss Andaru Dena Prasiwi
Field of Study	Chemistry
Thesis Advisor	Assistant Professor Prompong Pienpinijtham, Ph.D.

Accepted by the FACULTY OF SCIENCE, Chulalongkorn University in
Partial Fulfillment of the Requirement for the Master of Science

..... Dean of the FACULTY OF
SCIENCE

()

THESIS COMMITTEE

.....	Chairman
(Associate Professor VUDHICHAJ PARASUK, Ph.D.)	Thesis Advisor
.....	(Assistant Professor Prompong Pienpinijtham, Ph.D.)
.....	Examiner
(Professor SUMRIT WACHARASINDHU, Ph.D.)	External Examiner
.....	(Associate Professor Pimthong Thongnopkun, Ph.D.)

จุฬาลงกรณ์มหาวิทยาลัย
CHULALONGKORN UNIVERSITY

อันดาเร เดนา พราชีวี : เซอร์เฟซเอนฮานซ์รามานสแกตเตอริงโดยใช้คาร์บอนควอนตัมดอตซึ่งถูกดับฟลูออเรสเซนซ์เพื่อการตรวจวัดไอออนปรอท . (SURFACE-ENHANCED RAMAN SCATTERING USING FLUORESCENCE-QUENCHED CARBON QUANTUM DOTS FOR MERCURY ION DETECTION) อ.ที่ปรึกษาหลัก :
พร้อมพงศ์ เทียรพินิจธรรม

ไอออนของปรอท (mercury ion; Hg^{2+}) เป็นปัญหาที่ทำลายอย่างมาก เนื่องจาก Hg^{2+} มีความเป็นพิษสูงแม้ที่ความเข้มข้นต่ำ รวมไปถึงการสะสมทางชีวภาพที่ส่งผลต่อสุขภาพของมนุษย์ ในที่นี้เราได้เสนอวิธีการในการใช้ประโยชน์จากการดับการเรืองแสง (fluorescence quenching) ของคาร์บอนควอนตัมดอต (carbon quantum dots, CQDs) ร่วมกับเทคนิคเซอร์เฟซเอนฮานซ์รามานสแกตเตอริง (surface-enhanced Raman scattering, SERS) เพื่อตรวจวัด Hg^{2+} โดยอาศัยหลักการว่าคาร์บอนควอนตัมดอตมีการเรืองแสงที่เข้มซึ่งรบกวนการวัดด้วยเทคนิค SERS แต่เมื่อมี Hg^{2+} ในระบบจะสามารถดับการเรืองแสงของคาร์บอนควอนตัมดอตได้ จึงทำให้สามารถวัดสเปกตรัมจากเทคนิค SERS ได้ ในงานนี้ได้ทำการศึกษาสเปกตรัมจากเทคนิค SERS ของ rhodamine 6G (R6G) ร่วมกับคาร์บอนควอนตัมดอตและ Hg^{2+} (ความเข้มข้น 0.100-100 นาโนกรัมต่อลิตร) โดยสเปกตรัมของ R6G ถูกใช้เป็นตัวชี้วัดความเข้มข้นของ Hg^{2+} เมื่อเติม Hg^{2+} สเปกตรัมของ R6G มีการเปลี่ยนแปลงของความเข้มสัญญาณ ปริมาณ Hg^{2+} หาได้จากกราฟพล็อตกราฟเส้นตรงระหว่างความเข้มสัญญาณรามานของ R6G ที่ตำแหน่ง 615 cm^{-1} (I_{615}) กับความเข้มข้นของ Hg^{2+} โดยมีสัมประสิทธิ์สหสัมพันธ์ (R^2) เท่ากับ 0.963 ในช่วงความเข้มข้น 0.100-0.800 นาโนกรัมต่อลิตร ปริมาณ Hg^{2+} ต่ำสุดที่ตรวจวัดได้ (limit of detection, LOD) คือ 0.190 นาโนกรัมต่อลิตร ทั้งนี้ความจำเพาะในการตรวจวัดทดสอบโดยใช้ไอออนของโลหะต่าง ๆ เป็นไอออนก่อน เทคนิคที่พัฒนาขึ้นนี้มีความจำเพาะอย่างดีในการตรวจวัด Hg^{2+} และเทคนิคนี้ยังสามารถใช้กับตัวอย่างน้ำจริง เมื่อทดลองกับตัวอย่างน้ำแร่จะให้ค่า LOD ของ Hg^{2+} เท่ากับ 0.194 นาโนกรัมต่อลิตร และ R^2 เท่ากับ 0.935 ที่ความเข้มข้นในช่วง 0.100-0.800 นาโนกรัมต่อลิตร การตรวจสอบความถูกต้องของเทคนิคนี้ทดสอบโดยใช้เทคนิค Inductively Coupled Plasma Optical Emission Spectrometry (ICP-OES) เทคนิค SERS ที่พัฒนาขึ้นนี้ทำให้การเตรียมตัวอย่างง่ายขึ้น มีความไวและความจำเพาะในการตรวจวัดที่ดีขึ้น

จุฬาลงกรณ์มหาวิทยาลัย
CHULALONGKORN UNIVERSITY

สาขาวิชา เคมี
ปีการศึกษา 2563

ลายมือชื่อนิสิต.....
ลายมือชื่อ อ.ที่ปรึกษาหลัก.....

6172191823 : MAJOR CHEMISTRY

KEYWORD Surface-Enhanced Raman Scattering (SERS), Carbon Quantum Dots (CQDs), Fluorescence-quenched, Mercury ion (Hg^{2+})

Andaru Dena Prasiwi : SURFACE-ENHANCED RAMAN SCATTERING USING FLUORESCENCE-QUENCHED CARBON QUANTUM DOTS FOR MERCURY ION DETECTION. Advisor: Asst. Prof. Prompong Pienpinijtham, Ph.D.

Mercury ion (Hg^{2+}) is one of the most challenging problems due to its high toxicity at low concentration and bioaccumulative effects affecting human health. Herein, we propose a strategy to exploit the fluorescence quenching of carbon quantum dots (CQDs) combined with surface-enhanced Raman scattering (SERS) technique to detect Hg^{2+} . CQDs exhibit strong fluorescence emission interfering SERS measurement. However, with the presence of Hg^{2+} , fluorescence from CQDs can be quenched, and the SERS spectrum can be collected. In this work, SERS spectra of rhodamine 6G (R6G) incorporated with CQDs and Hg^{2+} (0.100–100 ng/L) were studied. The SERS spectra of R6G was used as an indicator for Hg^{2+} concentration. Upon the addition of Hg^{2+} , the SERS spectra of R6G showed changes in the intensity. To quantify Hg^{2+} , the Raman intensity of R6G at 615 cm^{-1} (I_{615}) was linearly plotted against the concentrations of Hg^{2+} with $R^2 = 0.963$ in the range of 0.100–0.800 ng/L. The limit of detection (LOD) of Hg^{2+} is 0.190 ng/L. Also, the selectivity was conducted by using various metal ions as interfering ion. The developed technique shows good selectivity to detect Hg^{2+} . This technique can be used for a practical application in a real water sample. The mineral drinking water sample was used as practical application with LOD of Hg^{2+} is 0.194 ng/L and $R^2 = 0.935$, ranging from 0.100–0.800 ng/L. Our developed technique was validated using Inductively Coupled Plasma Optical Emission Spectrometry (ICP-OES). This developed SERS technique provides a simple sample pretreatment, sensitivity, and good selectivity.

จุฬาลงกรณ์มหาวิทยาลัย
CHULALONGKORN UNIVERSITY

Field of Study: Chemistry

Student's Signature

Academic Year: 2020

Advisor's Signature

Year:

.....

ACKNOWLEDGEMENTS

I would like to thank the following people, without whom I would not have been able to complete this research, and without whom I would not have made it through my master's degree. Firstly, I would like to express my deep and sincere gratitude to my advisor Asst. Prof. Dr. Prompong Pienpinijtham, for the continuous support for the past two years of my study and the related research project, for his patience, motivation, and immense knowledge. His guidance and feedback helped me throughout this research project and writing this thesis. I could not have imagined having a better advisor and mentor for my study. I would like to extend my special thanks also to Prof. Dr. Sanong Ekgasit and Assoc. Prof. Dr. Kanet Wongravee that guided me so positively to widen my research from various perspectives and precious support to conduct this research.

I wish to show my appreciation to my thesis committee: Assoc. Prof. Dr. Vudhichai Parasuk, Prof. Dr. Sumrit Wacharasindhu, and Assoc. Prof. Dr. Pimthong Thongnopkun, for their insightful comments and encouragement.

I would like to sincerely thank my colleagues at the SRU research group, Chulalongkorn University, to stimulate discussions and helping me through the hard times.

Moreover, I gratefully acknowledge the financial support under ASEAN scholarship, Department of Chemistry, Chulalongkorn University and National Nanotechnology Center (NANOTEC), National Science and Technology (NSTDA), Ministry of Science and Technology, Thailand, through its Research Network NANOTEC (RNN) program.

Finally, I would like to thank my family for supporting me spiritually throughout writing this thesis and encouraging me all the time.

Andaru Dena Prasiwi

TABLE OF CONTENTS

	Page
ABSTRACT (THAI)	iii
ABSTRACT (ENGLISH).....	iv
ACKNOWLEDGEMENTS	v
TABLE OF CONTENTS.....	vi
LIST OF TABLES	1
LIST OF FIGURES	2
LIST OF ABBREVIATIONS.....	4
CHAPTER 1 INTRODUCTION	6
1.1 Problem and background.....	6
1.2 Objective.....	13
1.3 Scope	13
1.4 The benefit of this research	13
CHAPTER 2 THEORY	14
2.1 Raman Spectroscopy	14
2.2 Surface-enhanced Raman Scattering (SERS)	15
2.3 Mercury ions.....	17
2.4 Carbon Quantum Dots (CQDs).....	18
2.5 Rhodamine 6G (R6G).....	20
2.6 Limit of Detection (LOD).....	20
2.7 The Validation Method.....	21
CHAPTER 3 EXPERIMENT	23
3.1 Chemicals.....	23
3.2 Synthesis of silver nanoparticles (AgNPs)	23
3.3 Synthesis of carbon quantum dots (CQDs)	24
3.4 Sample preparation for SERS measurement.....	24

3.5 Hg ²⁺ detection in real water sample.....	25
3.6 Characterization techniques.....	25
3.6.1 UV–Visible spectroscopy.....	25
3.6.2 Scanning electron microscopy.....	25
3.6.3 Fluorescence spectrophotometer.....	26
3.6.4 Raman spectroscopy.....	26
3.6.5 Inductively coupled plasma-optical emission spectrometry.....	26
3.7 Data Analysis.....	27
CHAPTER 4 RESULTS AND DISCUSSION.....	28
4.1 The characterization of colloidal citrate-reduced silver nanoparticles.....	28
4.2 Spectroscopic studies of R6G and Hg ²⁺	30
4.3 Optical properties of the CQDs.....	32
4.4 Raman spectra of AgNPs, CQDs, and CQDs in the presence of Hg ²⁺	33
4.5 SERS detection of Hg ²⁺ using AgNPs.....	34
4.6 Optimization of R6G concentration in SERS measurement.....	37
4.7 SERS detection of Hg ²⁺ using CQDs incorporated with Rhodamine 6G.....	39
4.8 Selectivity of Hg ²⁺ detection.....	42
4.9 Determination of Hg ²⁺ in a mineral drinking water sample.....	43
4.10 Validation for Hg ²⁺ determination method.....	46
CHAPTER 5 CONCLUSIONS.....	48
REFERENCES.....	50
VITA.....	56

LIST OF TABLES

Table 1. 1 Conventional methods for Hg ²⁺ detection.....	8
Table 1. 2 SERS substrate for Hg ²⁺ detection.....	11
Table 4. 1 Band assignments of citrate	36
Table 4. 2 Basic types of vibrations and their description with Greek symbols	37
Table 4. 3 Band assignments of R6G Raman spectrum.....	39
Table 4. 4 Validation method for determination of Hg ²⁺	47



LIST OF FIGURES

Figure 1.1 A SERS strategy using fluorescence-quenched CQDs to detect Hg^{2+}	12
Figure 2.1 Energy level diagram involving Rayleigh scattering and Raman scattering	15
Figure 2.2 Localized surface plasmon resonance (LSPR).	16
Figure 2.3 A synthetic route using citric acid and ethylenediamine	19
Figure 2.4 Schematic illustration of CQDs fluorescence and quenching mechanism by Hg^{2+}	19
Figure 2.5 Molecular formula of R6G	20
Figure 3.1 Schematic illustration of sample preparation for SERS measurement.....	25
Figure 4.1 UV-visible spectrum of synthesized AgNPs colloid.	29
Figure 4.2 SEM image of AgNPs (a) x20.000, (b) x50.000, and (c) particle size of AgNPs	30
Figure 4.3 UV-visible spectrum of Hg^{2+}	31
Figure 4.4 UV-visible spectrum of R6G	31
Figure 4.5 UV-visible spectrum of synthesized CQDs	32
Figure 4.6 Fluorescence spectra of CQDs by using 346 nm excitation wavelength in the (a) presence and (b) absence of Hg^{2+} ($[\text{Hg}^{2+}] = 100 \text{ mg/L}$ in sample).....	33
Figure 4.7 Raman spectra of (a) AgNPs, (b) CQDs, and (c) CQDs in the presence of Hg^{2+} (100 ng/L).	34
Figure 4.8 Raman spectra of (a) AgNPs, (b) AgNPs with Hg^{2+} ($[\text{Hg}^{2+}] = 100 \text{ ng/L}$), (c) dried AgNPs, and (d) dried AgNPs with Hg^{2+} ($[\text{Hg}^{2+}] = 100 \text{ ng/L}$).	35
Figure 4.9 SERS spectra collected from R6G (10^{-4} M to 10^{-8} M) adsorbed on AgNPs, which were coupled with CQDs in the (a) presence and (b) absence of Hg^{2+} (100 ng/L).....	38
Figure 4.10 SERS spectra of R6G incorporated with CQDs and Hg^{2+} at different Hg^{2+} concentrations.	40
Figure 4.11 Plot of I_{615} against Hg^{2+} concentration (0.100-100 ng/L).....	41
Figure 4.12 The correlation of Hg^{2+} concentration (0.100–0.800 ng/L) and peak intensity of R6G at 615 cm^{-1}	42

- Figure 4.13** I_{615} measured from samples containing Hg^{2+} and interfering metal ions. The concentration of Hg^{2+} is 1.00 ng/L in the presence of 1% of another interfering metal ions.....43
- Figure 4.14** SERS spectra of R6G incorporated with CQDs and Hg^{2+} at different Hg^{2+} concentrations (0.100-100 ng/L) in mineral drinking water44
- Figure 4.15** Plot of peak intensity at 615 cm^{-1} (I_{615}) against Hg^{2+} concentration (0.1-100 ng/L) in mineral drinking water45
- Figure 4.16** The correlation of Hg^{2+} concentration (0.100–0.800 ng/L) and peak intensity of R6G at 615 cm^{-1} in mineral drinking water46



LIST OF ABBREVIATIONS

ν	: stretching
δ	: bending
ρ	: rocking
ω	: wagging
τ	: twisting
sym	: symmetric
asym	: antisymmetric
AgNPs	: silver nanoparticles
AuNPs	: gold nanoparticles
MNPs	: metal nanoparticles
SERS	: surface-enhanced Raman scattering
LSPR	: localized surface plasmon resonance
CQDs	: carbon quantum dots
R6G	: rhodamine 6G
Hg ²⁺	: mercury ions
SEM	: scanning electron microscopy
ICP-MS	: inductively coupled plasma mass spectrometry
AFS	: atomic fluorescence spectrometry
AAS	: atomic absorption spectrometry
GC-MS	: gas chromatography mass spectrometry
UV-Visible	: ultraviolet-visible

IR	: infrared
DI water	: deionized water
LOD	: limit of detection
M	: molar
mm	: millimetre
mL	: millilitre
mg/L	: miligram per litre
$\mu\text{g/L}$: microgram per litre
ng/L	: nanogram per litre
min.	: minutes



CHAPTER 1

INTRODUCTION

1.1 Problem and background

Raman spectroscopy is an important analytical technique for chemical and biological analysis due to the extensive amount of information obtained from the molecular structures, surface processes, and reactions at the interface.[1-3] Raman spectroscopy provides fingerprint-type information on the composition and arrangement of defined molecules and material identification.[4] Raman scattering happens when energy is transferred from photon to the molecule or vice versa. The scattered photon has less or more energy than the incident photon.[5] Raman signal is very weak as it requires powerful sources and sensitive detectors. Raman spectroscopy has been less widely used due to its relatively weak signal and low sensitivity, which a small amount of samples is hard to perform, and fluorescence interference. The detection of a very weak Raman signal is often obstructed by fluorescence background. It is common for a weak Raman signal to be buried within a broad and intense fluorescence background. Therefore, quenching has been used to deplete the emitting state and thereby minimize fluorescence.[6] This research aimed to used the weakness of fluorescence in Raman spectroscopy to detect mercury ions.

Heavy metals are persistent in the environment, contaminate the food chains, and induce various health problems due to their toxicity. Long-term exposure to heavy metals in the environment is real damage to living organisms.[7] Mercury ions (Hg^{2+}) is one of the most toxic heavy metal ions due to their deadly toxicity at low concentration and bioaccumulative effect in ecosystems.[8, 9] The world health

organization (WHO) suggested 6 $\mu\text{g/L}$ of inorganic mercury as the guideline tolerable value for mercury in drinking water.[10] Mercury ions, particularly water-soluble Hg^{2+} , can easily pass through skin, respiratory, and gastrointestinal tissues, leading to DNA damage, mitosis impairment, and permanent damage to the central nervous system.[11] Human activities have nearly tripled the amount of mercury in the atmosphere, and the atmospheric burden is increasing by 1.5 percent per year.[12]

In recent years, analytical methods have been used to detect Hg^{2+} . Mao, *et al.*[13] used atomic fluorescence spectrometry (AFS) and inductively coupled plasma mass spectrometry (ICPMS) to detect organomercury in sediment samples collected from the Florida Everglades and a Canadian wetland. The sediment samples were kept in a cooler during transport and were transferred into a refrigerator (4 $^{\circ}\text{C}$). Organomercury species in sediment were isolated following the extraction, digestion, high enrichment capacity of purge, and trap with aqueous phenylation derivatization. Then, monomethyl mercury (MeHg) and monoethyl mercury (EtHg) products were detected by AFS and ICP-MS. Based on the results, detection limits were 0.03 ng/L for both MeHg and EtHg by AFS. Then, detection limits were 0.02 and 0.01 ng/L for MeHg and EtHg with ICP-MS, respectively.

Hippler, *et al.*[14] used gas chromatography coupled with mass spectrometry (GC-MS) to determine methyl mercury (MeHg) in blood samples collected from workers of a mercury recycling plant. The samples were transferred into tubes containing sodium citrate as anti-coagulant, stored at 6 $^{\circ}\text{C}$ in a refrigerator, extracted, derivatized, and measured using GC-MS. The lowest concentration that can be detected was 0.5 $\mu\text{g/L}$.

Lemos, *et al.*[15] used atomic absorption spectrometry (AAS) to detect Hg^{2+} in shrimp collected from Muribeca in Todos os Santos Bay, Bahia, Brazil. Samples were digested, adjusted the pH with a NaOH solution, and preconcentrated before analyzed by AAS. The assay presented a limit detection of 0.011 $\mu\text{g/L}$.

Lim, *et al.*[16] used a colorimetric method that produces DNAzymes by rolling circle amplification (RCA) to detect Hg^{2+} in tap drinking water. Samples were added to the mixed RCA solution containing a circular DNA template. The colorimetric probe exhibits a high sensitivity of 3.6 $\mu\text{g/L}$.

However, these methods are often limited by sensitivity, low selectivity, high-cost instruments, complex procedures, and samples pretreatment. Moreover, these methods are difficult to be used in real-time detection. Table 1.1 shows the conventional techniques used to detect Hg^{2+} with their detection limit.

Table 1.1 Conventional methods for Hg^{2+} detection

Year	Author	Technique	Detection Limit
2008	Mao, <i>et al.</i>	AFS	0.03 ng/L
		ICP-MS	0.01 and 0.02 ng/L
2009	Hipler, <i>et al.</i>	GC-MS	0.5 $\mu\text{g/L}$
2014	Lemos, <i>et al.</i>	AAS	0.011 $\mu\text{g/L}$
2019	Lim, <i>et al.</i>	Colorimetric	3.6 $\mu\text{g/L}$

Surface-enhanced Raman scattering (SERS) is a powerful sensing technology using metal nanoparticles (MNPs) as a substrate, such as silver and gold, to enhance the signal of analytes. It is one of the most sensitive detection technologies. It has

received wide recognition in many industries because of its high sensitivity, noninvasiveness, high resolution, and fingerprint information about the chemical structure.[17-20] Metal ions, cannot undergo Raman scattering due to lack of vibrational transition. Accordingly, one of the main challenges for Hg^{2+} detection is to develop an effective platform by fabricating SERS substrate, generating enhancement of Raman signal. Several previous works have been reported the modification of SERS substrate for Hg^{2+} detection. For instance, Ding, *et al.*[21] fabricated gold nanoparticles (AuNPs)/reduced graphene oxide (rGO) heterojunctions on SiO_2/Si substrate *via* seed-assisted growth process. The SERS substrates has been utilized for trace analysis of Hg^{2+} *via* thymine- Hg^{2+} -thymine coordination with a limit of detection can reach 0.02 ng/L for Hg^{2+} .

Song, *et al.*[22] reported SERS sensor by immobilizing thymines-component oligonucleotide probes labeled with a Cy5 dye on the 3'-end and a -SH on the 5'-end functionalized silver nanorods (AgNRs) array as SERS substrate. The SERS sensor responds to the specific chemical bonding between thymine and Hg^{2+} , which causes the previous flexible single strand of an oligonucleotide probe to change into a rigid and upright double-chain structure. Thus, the Cy5 dyes are far away from the SERS substrate, resulting in a noticeable decrease of SERS intensity of Cy5. The detection limit of 0.03 ng/L is obtained.

Zeng, *et al.*[23] have been demonstrated that 2,5-Dimercapto-1,3,4-thiadiazole (DMcT) functionalized Au@Ag nanoparticles (NPs) were constructed as a label-free SERS probe. DMcT coordinated on the surface of Au@Ag NPs as a bidentate ligand with both the thiocarbonyl sulfur atoms while the nitrogen atoms on the different

sides of the molecule were devoted to Hg^{2+} recognition. The strong coordination between Hg^{2+} and nitrogen atoms can be detected as low as 2 ng/L.

Guselnikova, *et al.*[24] utilized surface plasmon-polariton (SPP) supporting gold gratings in combination with diazonium grafted 4-ethynylphenyl groups, which is undergone the sunlight-induced thiol-yne reaction with mercaptosuccinic acid (MSA) in the presence of Eosine-Y as SERS platform for Hg^{2+} detection. The limit of detection (LOD) can reach 10^{-10} M (0.027 $\mu\text{g/L}$).

Zhao, *et al.*[25] reported SERS sensor by decorating the inner wall of capillary with 4,4'-dipyridyl (Dpy) functionalized silver nanoparticles (AgNPs). In the presence of Hg^{2+} , the Dpy molecules separated from the surface of AgNPs and coordinated with Hg^{2+} , resulting in a decrease in the SERS signal. The limit of detection (LOD) was determined to be 0.1 $\mu\text{g/L}$.

Hao, *et al.*[26] conducted a study on the determination of Hg^{2+} in water by SERS based on acriflavine functionalized AgNPs. The interaction of acriflavine with AgNPs was inhibited because citrate reduced Hg^{2+} to Hg and formed Ag-Hg on the AgNPs surface, resulting in a decrease of SERS intensity of acriflavine. The detection limit was as low as 0.28 $\mu\text{g/L}$.

Table 1.2 SERS substrate for Hg²⁺ detection

Year	Author	Substrate	LOD of Hg ²⁺
2013	Ding, <i>et al.</i>	AuNPs/rGO heterojunctions on SiO ₂ /Si	0.02 ng/L
2017	Song, <i>et al.</i>	AgNRs immobilized oligonucleotide with Cy5 dye on the 3'-end and -SH on the 5'-end	0.03 ng/L
2017	Zeng, <i>et al.</i>	Au@Ag NPs with DMcT	2 ng/L
2019	Guselnikova, <i>et al.</i>	Au gratings combined with diazonium grafted 4-ethynylphenyl and MSA	0.027 µg/L
2020	Zhao, <i>et al.</i>	AgNPs functionalized Dpy	0.1 µg/L
2020	Hao, <i>et al.</i>	AgNPs modified with acriflavine	0.28 µg/L

In this work, we proposed to use the drawback of fluorescence on SERS to be a fundamental key for Hg²⁺ detection. Silver nanoparticles (AgNPs) were chosen to be a SERS substrate. However, only AgNPs cannot detect Hg²⁺ because no molecular bond of Hg²⁺, causing no vibration to produce Raman signal. Therefore, we functionalized the surface of AgNPs with rhodamine 6G (R6G) to enhance Raman signal intensity. Also, carbon quantum dots (CQDs) generates fluorescence noise that can be quenched by Hg²⁺. Therefore, the coupling between AgNPs, R6G, and CQDs is needed to detect Hg²⁺. Moreover, we aimed to quench the fluorescence of CQDs by Hg²⁺ to observe SERS signals of Raman Dye. R6G is a highly fluorescent rhodamine family dye. It can be used as a tracer dye and SERS signals of Raman dye. In this work, R6G is used as an indicator for Hg²⁺ based on the shifting intensity of

the R6G peak. As shown in Figure 1.1a, citrate-coated silver nanoparticles attracted R6G molecules to assemble on its surface structures, resulting in SERS signal enhancement. However, in Figure 1.1b, CQDs existence in the AgNPs and R6G system generates intense fluorescence noise leading to a decrease of SERS signal. Specifically, in Figure 1.1c, the addition of Hg^{2+} can quench the fluorescence of CQDs in the system, producing the increase of SERS signal back.

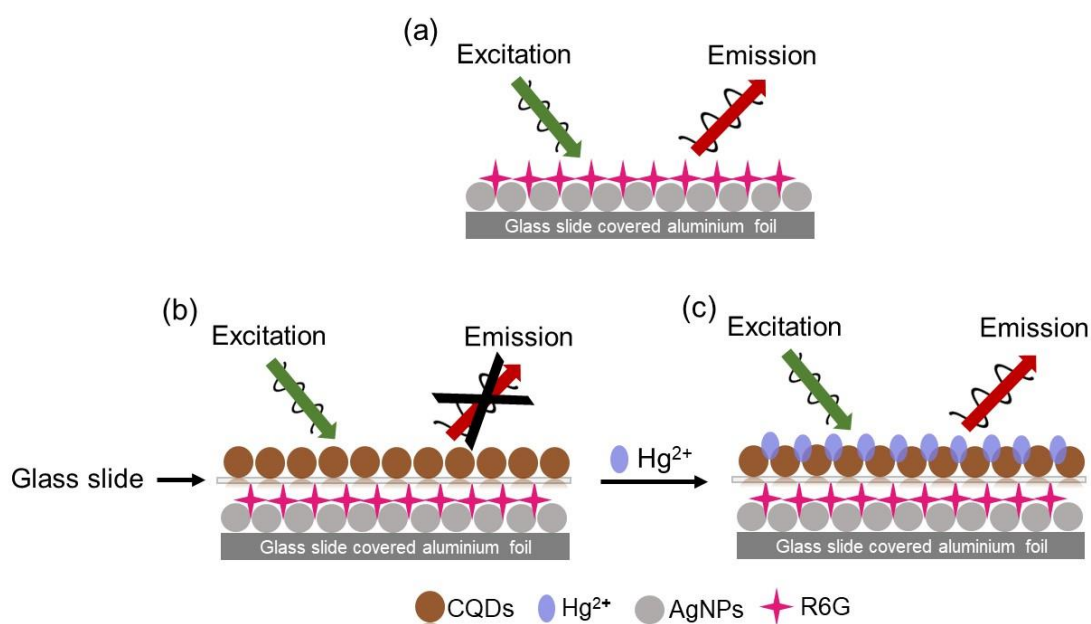


Figure 1.1 A SERS strategy using fluorescence-quenched CQDs to detect Hg^{2+}

1.2 Objective

The objective of this work is to develop a sensitive, selective, and convenient SERS method by using fluorescence-quenched CQDs coupling with AgNPs and R6G for Hg^{2+} detection.

1.3 Scope

1. The detection of different concentrations of Hg^{2+} by using the developed technique.
2. The SERS spectra of R6G as an indicator for Hg^{2+} by using fluorescence-quenched CQDs are investigated.
3. The amount of Hg^{2+} spiked on the real water sample is quantified using the developed technique.

1.4 The benefit of this research

The developed technique based on the fluorescence-quenched will be used for Hg^{2+} detection under SERS technique.

CHAPTER 2

THEORY

2.1 Raman Spectroscopy

Raman spectroscopy is a nondestructive analytical technique. This technology can detect vibrational and rotational spectra of molecules excited by a laser in real-time and provide molecular specificity, structural characteristics, and relatively simple spectral fingerprint information.[27] Raman scattering is a fundamental form of molecular spectroscopy. With infrared (IR) absorption, Raman scattering is used to obtain information about the structure and properties of molecules from their vibrational transitions. IR absorption involved in the resonant interaction with the change in the dipole moment of molecule to its vibrational motion. By contrast, Raman scattering involved with the change in the polarizability of a molecule to its vibrational motion. Due to the light interaction with matter, an electric dipole within molecules is induced since the atoms become polarized. The light scattered consists of both Rayleigh scattering and Raman scattering. Figure 2.1 (a). Rayleigh scattering corresponds to the light scattered at the frequency of the incident radiation (ν_0). Whereas the Raman radiation is shifted in the frequency of the incident radiation by the vibrational energy that is gained or lost in the molecule, indicated in Figure 2.1 (b). The scattering is called Stokes Raman, if the molecule gains vibrational energy and photon lose energy, the frequency of photon will be red-shifted (shifted to a lower frequency), which the photons in the excited state adsorb the incident light with frequency (ν_0). Then, Figure 2.1 (c). The process is known as anti-Stokes Raman scattering, if the molecule loses vibrational energy and photons gain energy, the frequency of photon will be blue-shifted (shifted to a higher frequency).[28, 29]

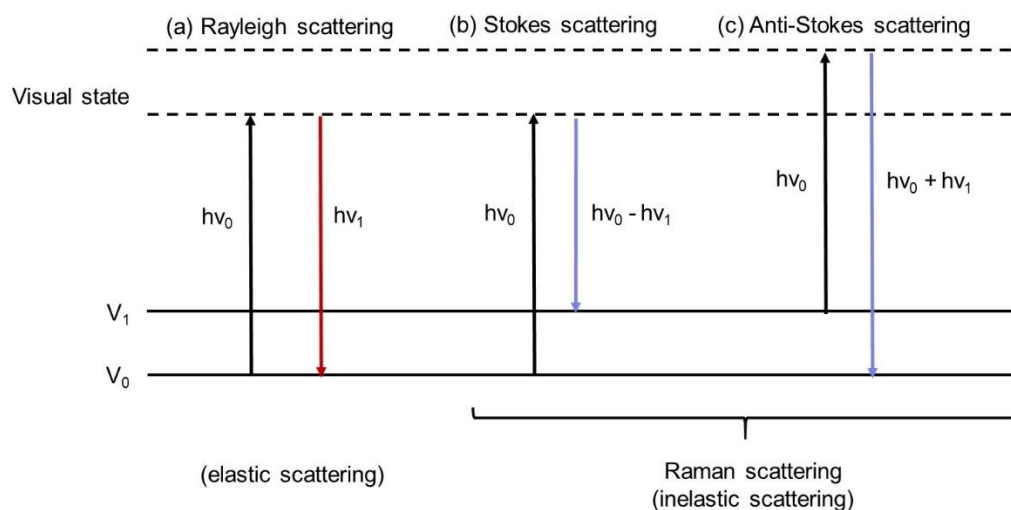


Figure 2.1 Energy level diagram involving Rayleigh scattering and Raman scattering.

Raman spectroscopy offers the advantages of being generally non-destructive, obtains spectra rapidly, and has no a major problem of interference from water. The disadvantage is that Raman scattering has low scattering efficiency. Surface-enhanced Raman scattering (SERS) is used to improve the process sensitivity. The Raman effect is inherently weak, with only ~ 1 in 10^8 photons from excitation source being effective, causing the detection of low concentration and a small amount of samples is hard to perform. The spectra are easily overwhelmed by broadband fluorescence. The effect of fluorescence can be eliminated by quenching the fluorescence.[30-33]

2.2 Surface-enhanced Raman Scattering (SERS)

Surface-enhanced Raman scattering (SERS) is a commonly used sensing technique, in which Raman scattering signals are greatly enlarged when the molecules were absorbed on the rough metal surface or metal nanoparticles such as silver and gold. SERS effect has attracted steady interest and has been used to detect and provide fingerprint information of analytical molecules at very low concentrations.

The enhanced Raman scattering from molecules arises in two ways: namely electromagnetic (EM) enhancement based on electromagnetic field enhancement on the metal surface and chemical (CE) enhancement based on charge transfer between the metal and molecule. The EM enhancement is defined as the collective oscillation of the conduction free electrons on the surface of metal nanoparticles, which is the so-called localized surface plasmon resonance (LSPR) in Figure 2.2.[34-39]

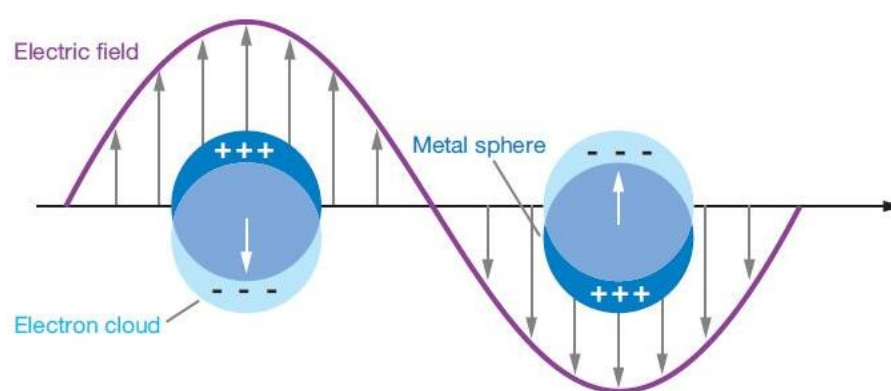


Figure 2.2 Localized surface plasmon resonance (LSPR).[40]

When the electrons in metallic nanoparticles are driven by the incident light is absorbed by the nanoparticles. Some of these photons will be released with the same frequency and energy in all directions, which is known as the process of scattering. Meanwhile, some of these photons will be converted into vibrations, which is referred to as absorption. Therefore, LSPR is a combined effect of scattering and absorption in the optical extinction spectra.[41] LSPR induced by incident light and free electrons around metal nanoparticles can form “hotspots” to enhance Raman scattering signals largely. It is well known that the “hotspots” are generally formed in nanogaps among noble metal nanoparticles. Silver and gold nanoparticles are the most widely used materials in SERS substrates due to their localized surface plasmon resonance (LSPR)

properties, which cover a wide wavelength range in the visible region. [42-46] It is critical for SERS analysis to fabricate the substrates with high enhancement performance, good uniformity, excellent reproducibility, and reusability. Several methods have been developed for the fabrication of substrates by focusing on the structural properties of SERS substrates with optimal enhancement properties. The SERS enhancement factor depends on several factors, such as metal nanoparticles size, shape, interparticles distance, and general arrangement. The fabrication of SERS substrates increased charge-transfer processes between a substrate and a sample molecule contributing to more enhanced SERS signals for sample detection. In this work, AgNPs was used as metal nanoparticles because of the impeccable physical and chemical qualities, can be easily prepared using few chemicals and simple procedure.[47, 48]

2.3 Mercury ions

Mercury is highly toxic to human health, giving a particular threat to all living organisms along the food chain of a given ecosystem become contaminated. Mercury occurs naturally and exists in various forms: *elemental* (or metallic), *inorganic* (e.g., mercuric chloride), and *organic* (e.g., methyl- and ethylmercury). These forms have different toxicities and implications for health.[49] Liquid of elemental mercury can vaporize and stay for up to a year in the atmosphere, which it can transport and deposit globally. Mercury vapors are colorless and odorless. It eventually reserves in the sediment of lakes, rivers, or bays where it is converted into methylmercury, absorbed by phytoplankton, ingested by zooplankton and fish.[50] Aside from natural activities, industrial processes involved in mining and petrochemicals, or other human activities such as the use of fungicidal sprays, household bleach, acid, and caustic

chemicals, also have the potential to release mercury. Human toxicity varies with the form of mercury, the dose, and the rate of exposure. The target organ for inhaled mercury vapor (Hg^0) is primarily the brain. Mercurous (Hg_2^{2+}) and mercuric salts (Hg^{2+}) chiefly damage the gut lining and kidney, while methyl mercury is widely distributed throughout the body. Once mercury is absorbed, it has a very low excretion rate. A major proportion of what is absorbed accumulates in the kidneys, neurological tissue, and the liver. All forms of mercury are toxic, and their effects include gastrointestinal toxicity, neurotoxicity, and nephrotoxicity.[11, 51-53] Up until now, there have been reports based on carbon quantum dots (CQDs) exhibiting good fluorescence showed responses to Hg^{2+} . For the design of a sensitive, selective, and convenient SERS sensor for the detection of Hg^{2+} , we utilized Hg^{2+} as a quencher of CQDs fluorescence for a promising application of Hg^{2+} detection in SERS. The fluorescence quenching is important for maximizing the use of SERS enhancement.

2.4 Carbon Quantum Dots (CQDs)

Carbon quantum dots (CQDs) are fluorescent carbon nanoparticles with a size less than 10 nm comprising graphitic cores surrounded by varied surface functional units.[54, 55] The bottom-up hydrothermal of CQDs involved the pyrolysis or carbonization of small organic molecules, for example, citric acid and ethylenediamine. Specifically, the formation of CQDs undergoes condensation, polymerization, and carbonization.[56] The reaction formed a chain by condensing citric acid and ethylenediamine, which amine from ethylenediamine was protonated by hydrogen from citric acid to form ammonium salt. Wherein, the molecules formed polymer-like CQDs. Then, the polymer-like CQDs were carbonized to form CQDs

shown in Figure 2.3. Thus the surface of CQDs is attached to a lot of pending carboxylate groups.[57]

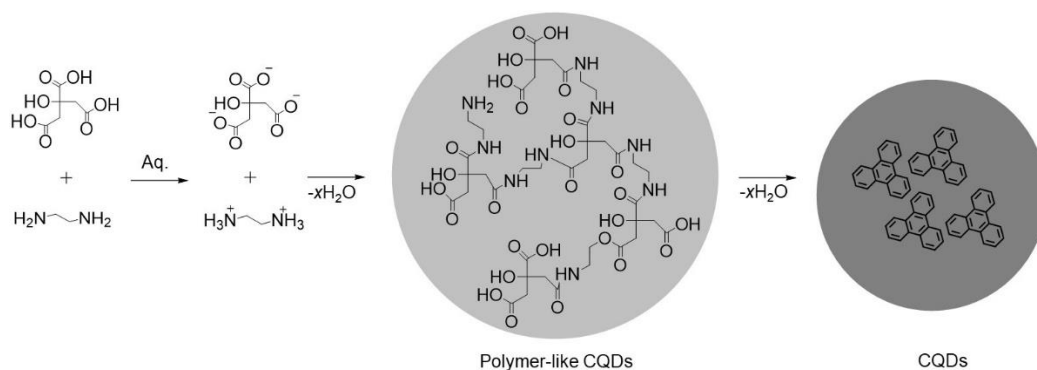


Figure 2.3 A synthetic route using citric acid and ethylenediamine.

The CQDs selectivity may be ascribed to the fact that Hg^{2+} has a stronger affinity towards the rich carboxylic group on the surface of CQDs in Figure 2.4. The as-prepared CQDs colloid exhibits strong fluorescence emission, which can be quenched by Hg^{2+} effectively due to an effective electron or energy transfer process.[58] CQDs have been applied as a sensing platform for mercury ions due to their broad color range, fluorescence brightness, chemical stability, biocompatibility, and low cytotoxicity, low cost, and readily available reagents, and simple synthesis procedures.[59-64]

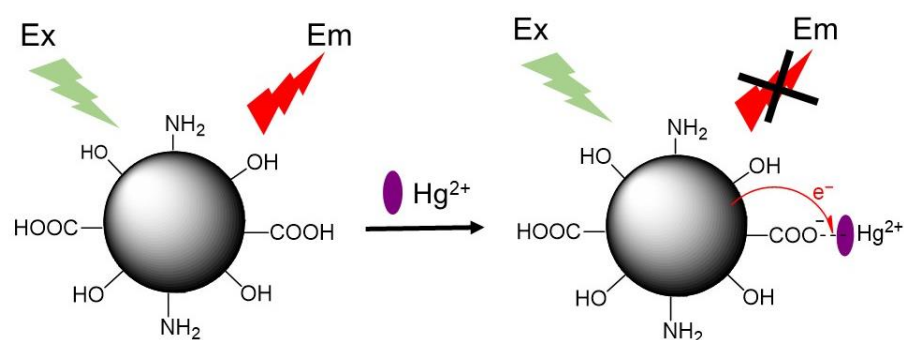


Figure 2.4 Schematic illustration of CQDs fluorescence and quenching mechanism by Hg^{2+} .

2.5 Rhodamine 6G (R6G)

Rhodamine 6G (R6G), containing two functional groups, a dibenzopyrene xanthene and a carboxyphenyl group titled about 90° with respect to xanthene ring, exhibits a boost of Raman intensity and high fluorescent yield, so this molecule has been widely used as SERS probes.[65] It was one of the first molecules used for single-molecule SERS studies with enhancement as large as 10^{14} to 10^{15} . It has been demonstrated that the SERS enhancement factor is closely related to the plasmon resonance of nanoparticle, laser excitation wavelength, and molecular resonance. Rhodamine 6G (R6G) has been chosen in this study because of its active role in SERS.[66, 67] In this work, R6G is used as an indicator of Hg^{2+} , based on the alteration of R6G peak intensity.

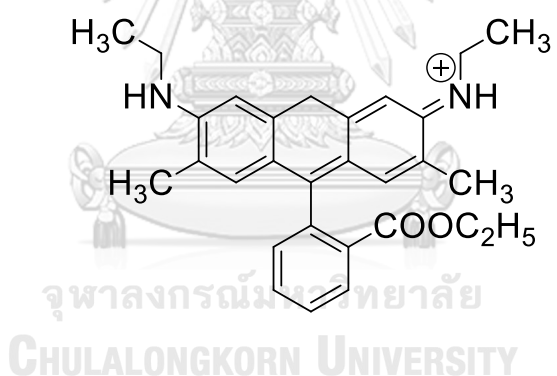


Figure 2.5 Molecular formula of R6G

2.6 Limit of Detection (LOD)

The limit of detection (LOD), which is defined as the smallest amount or concentration of particular substance that can be reliably detected in a given type of sample or medium by a specific measurement process. LOD has always been an indispensable performance for deciding the reliability of qualitative and also quantitative measurements.[68] The estimation of LOD is closely linked to the calibration curve method used. Linear regression-based calibration curve methods

may be employed when focusing on instruments operating in the linear range of the univariate sensor. The calibration curve is the graphical plot of the calibration function. The plot relates the signal to the analyte amount or concentration. Then, the resulting calibration can be used to estimate LOD.[69-71]

LOD is usually determined by means of data extracted from calibration curves. According to the IUPAC definition, the LOD for a given element is the concentration producing a net line intensity equal to three times the standard deviation of the background:

$$LOD = [3.3 \times \frac{\sigma}{s}] \quad (1)$$

3.3 = Expansion factors

σ = Standard deviation

s = Slope

Where s is the slope of the calibration curve for the specific atomic emission, also called sensitivity, at the lowest measured concentration. The value of σ is the standard deviation of different measurements on the least concentrated sample.[72]

2.7 The Validation Method

Nowadays, the validation method has been intensified to achieve a high level of quality. The criteria used to obtain results in the area in analytical chemistry are progressively more intense due to an increasing necessity to ensure that the results obtained from researches present safety and reliability.[73] This process aims to confirm that the method applied is compatible. Standard methods used outside the traditional scoped, extensions, and modifications of standard methods must be

validated with equipment and instruments within specification, working correctly, and properly calibrated.[74] A technique that is appropriated for the determination of metallic elements is the inductively coupled plasma mass spectrometry (ICP-MS). This methodology is very promising in the area of environmental studies since several elements can be determined using this technique, which is highly sensitive for ion detection.[75-77]



CHAPTER 3

EXPERIMENT

3.1 Chemicals

Citric acid monohydrate ($C_6H_8O_7 \cdot H_2O$), ethylenediamine ($C_2H_4(NH_2)_2$), and mercury (II) chloride ($HgCl_2$) were purchased from Merck. Silver nitrate ($AgNO_3$), trisodium citrate dihydrate ($Na_3C_6H_5O_7 \cdot 2H_2O$), and rhodamine 6G (R6G) were purchased from Aencore Chemical Co., Ltd., Carlo Erba Reagents S.A.S., and Sigma Aldrich, respectively. Cadmium sulphate ($CdSO_4 \cdot 8H_2O$), calcium chloride ($CaCl_2$), aluminium sulfate ($Al_2(SO_4)_3$), zinc chloride ($ZnCl_2$), copper (II) sulphate ($CuSO_4 \cdot 5H_2O$), nickel (II) nitrate hexahydrate ($Ni(NO_3)_2 \cdot 6H_2O$), and cobalt chloride hexahydrate ($CoCl_2 \cdot 6H_2O$) were purchased from LobaChemie Pvt. Ltd., Sigma Aldrich, Kurusapa Business Organization, Quality Reagent Chemical Product, Ajax Finechem Pty. Ltd., PanReac AppliChem, and J.T. Baker Chemical Co., respectively. Potassium sulfate (K_2SO_4) and manganese (II) sulfate tetrahydrate ($MnSO_4 \cdot 4H_2O$) were purchased from Merck. Iron (II) sulphate ($Fe_2SO_4 \cdot 7H_2O$) and iron (III) chloride ($FeCl_3$) were purchased from Carlo Erba Reagents S.A.S. Lead (II) chloride ($PbCl_2$) and stannous chloride dihydrate ($SnCl_2 \cdot 2H_2O$) were purchased from Fluka. All chemicals were used without any further purification. Milli-Q-system (Millipore, Bedford, MA, USA), and deionized water were employed as a solvent.

3.2 Synthesis of silver nanoparticles (AgNPs)

The preparation of silver nanoparticle colloid was synthesized by the reduction of $AgNO_3$ with $Na_3C_6H_5O_7$. [78] Briefly, 90 mg of silver nitrate was dissolved in 500 mL milli-Q water and heated until its boiling. A solution of 1% trisodium citrate (10

mL) was added dropwise into a boiling silver nitrate solution under a vigorous stir. The mixture was kept boiling and constantly stirring for 1 hour. The mixture color changed from colorless to a milky grey, indicating the formation of silver nanoparticles. The mixture was cooled down to room temperature. The flask containing the mixture was wrapped by aluminum foil to prevent light degradation of the colloid.

3.3 Synthesis of carbon quantum dots (CQDs)

CQDs was prepared according to a bottom-up hydrothermal method.[57] Typically, 5.0 g citric acid and 1.5 mL ethylenediamine were dissolved in 10 mL milli-Q. Then, the solution was transferred to a Teflon-lined stainless autoclave and heated at 165 °C for 150 min. The color of mixture slowly turned from colorless to clear brownish. After that, the mixture was cooled down to room temperature. The obtained clear brownish colloid was stored at 4 °C for further characterization and use.

3.4 Sample preparation for SERS measurement

The prepared AgNPs were mixed with a solution of R6G (1.0×10^{-7} M) in the volume ratio of 1:1 by using vortex mixer and ultrasonic treatment. The mixture was dropped and dried on a glass slide covered with an aluminum foil. After that, the clear glass slide was placed upon the dried AgNPs film. Then, the synthesized CQDs were separately mixed with different solutions of Hg^{2+} concentrations (0.100, 0.200, 0.400, 0.500, 0.600, 0.800, 1.00, 5.00, 10.0, 50.0, and 100 ng/L) in the volume ratio 1:1 by using a vortex mixer and ultrasonic treatment. Then, the mixed solution of CQDs and Hg^{2+} were dropped on the clear glass slide above the dried droplet of AgNPs and R6G

mixture. After that, a double cover slips (thickness = 1 mm) was placed on the clear slide and on top of CQDs to establish the flat liquid surface of the droplet of CQDs.



Figure 3.1 Schematic illustration of sample preparation for SERS measurement.

3.5 Hg²⁺ detection in real water sample

To demonstrate the practicability of this developed method, solutions of Hg²⁺ concentrations were spiked in mineral water samples to obtain the samples with the final Hg²⁺ concentrations of 0.100, 0.200, 0.400, 0.500, 0.600, 0.800, 1.00, 5.00, 10.0, 50.0, and 100 ng/L. These spiked samples were mixed with CQDs with volume ratio 1:1 by using a vortex mixer and ultrasonic treatment. Then, the sample preparation and SERS measurement were conducted as the same as in Section 3.4.

3.6 Characterization techniques

3.6.1 UV–Visible spectroscopy

UV–Visible spectroscopy was used to examine the plasmon extinction of synthesized AgNPs, the optical properties of CQDs, R6G, and Hg²⁺. Milli-Q water was used as a blank. Plasmon extinction spectrum of AgNPs, optical properties spectrum of CQDs, R6G, and Hg²⁺ was characterized by GENESYS 10S UV–Vis spectrometer ranging from 200–800 nm.

3.6.2 Scanning electron microscopy

The morphology of synthesized AgNPs was investigated by scanning electron microscopy (SEM) techniques. A carbon tape was attached to an aluminum stub. The synthesized AgNPs sample was dropped on a carbon tape and then vacuumed until

it's dried before imaging. SEM micrographs of synthesized AgNPs sample were analyzed by a scanning electron microscope (SEM, JEOL JSM-6510) conducted at 20 kV under a high vacuum mode.

3.6.3 Fluorescence spectrophotometer

The fluorescence of CQDs and the fluorescence of CQDs quenched by Hg^{2+} were obtained using a fluorescence spectrophotometer. CQDs were diluted 10000x before measuring. The used Hg^{2+} concentrations were ranging from 0.100-100 ng/L. A glass cuvette was used as a sample container. Fluorescence spectra of CQDs were performed using Cary Eclipse fluorescence spectrophotometer (agilent) under 346-nm excitation wavelength.

3.6.4 Raman spectroscopy

Raman spectroscopy was used to examine SERS spectra for Hg^{2+} detection. SERS spectra were recorded using DXR Raman microscope (Thermo scientific) with a 532-nm excitation lasers at a laser power of 10 mW using a 25- μm pinhole aperture, and an exposure time of 2 seconds with an accumulation number of 32. Each sample was measured by focusing on the dried droplet of AgNPs and R6G with 15 repeats.

3.6.5 Inductively coupled plasma-optical emission spectrometry

Inductively coupled plasma was used to measure Hg^{2+} concentration that was spiked on deionized water and mineral drinking water. Hg^{2+} concentration of 0.100 mg/L was spiked on deionized water and mineral drinking water to validate our method. The Hg^{2+} concentration was performed using high-resolution Inductively Coupled Plasma Optical Emission Spectrometry (ICP-OES, PlasmaQuant PQ 9000 Elite) by the Institute of Environmental Research.

3.7 Data Analysis

The limit of detection (LOD) was used to analyze the lowest concentration of Hg^{2+} in the sample, which can be quantitatively determined with suitable precision and accuracy. LOD is calculated based on the standard deviation (SD) of response (σ) and slope (s) of the calibration curve. The standard curve was constructed by plotting the concentration of Hg^{2+} on the X-axis ranging from 0.100, 0.200, 0.400, 0.500, 0.600, and 0.800 ng/L and R6G peak intensities at 615 cm^{-1} on the Y-axis. Then, plot a linear curve to assume the R6G peak intensities at 615 cm^{-1} is directly proportional to the Hg^{2+} concentration. After that, the regression function was used to carry out a regression analysis by selecting the data of X and Y variables. The regression function yields 3 outputs: regression statistics, ANOVA, and coefficients. ANOVA gives the level of variability within the regression model and coefficient, including the slope (s) of the curve and the standard deviation (σ) of the Y-intercept. The LOD can be calculated according to the equation 1:

$$LOD = \left[3.3 \times \frac{\sigma}{s} \right] \quad (1)$$

3.3 = Expansion factors

σ = Standard deviation

s = Slope

CHAPTER 4

RESULTS AND DISCUSSION

4.1 The characterization of colloidal citrate-reduced silver nanoparticles

According to Lee and Meisel method, the synthesized AgNPs colloid was prepared by reducing AgNO₃ with trisodium citrate (Na₃C₆H₅O₇) at its boiling point.[78] The addition of Na₃C₆H₅O₇ as a reducing agent changed the mixture color from colorless to a milky grey (inset in Figure 4.1). In Figure 4.1, AgNPs exhibit a UV-visible absorption maximum at 413 nm, attributing to the in-plane dipole plasmon resonance. It indicates the presence of spherical or roughly spherical AgNPs with an average particle size of approximately 50 nm. The broad peak at 413 nm also suggests a broad size distribution of particle size.[79] Moreover, the out-of-plane quadruple plasmonic band as a shoulder at 350 nm indicates the formation of large particles.[80, 81]

The morphology of synthesized AgNPs was evaluated by SEM. Based on the SEM image in Figure 4.2, the AgNPs were a spherical shape with a diameter size of 62.38 ± 12.32 nm. The big size variation could be due to the agglomeration of individual particles into larger particles due to the magnetic nature of silver. As magnetic NPs had high surface energy, and in order to minimize their energy, they could agglomerate to form larger secondary particles under the effect of magnetization.[82] AgNPs may results in different sizes and shapes, depending on several factors. The most important factors are the reaction temperature and the amount of reducing agent. Thus, the optical and electronic features of AgNPs are mostly influenced by the shape of nanoparticles.[83]

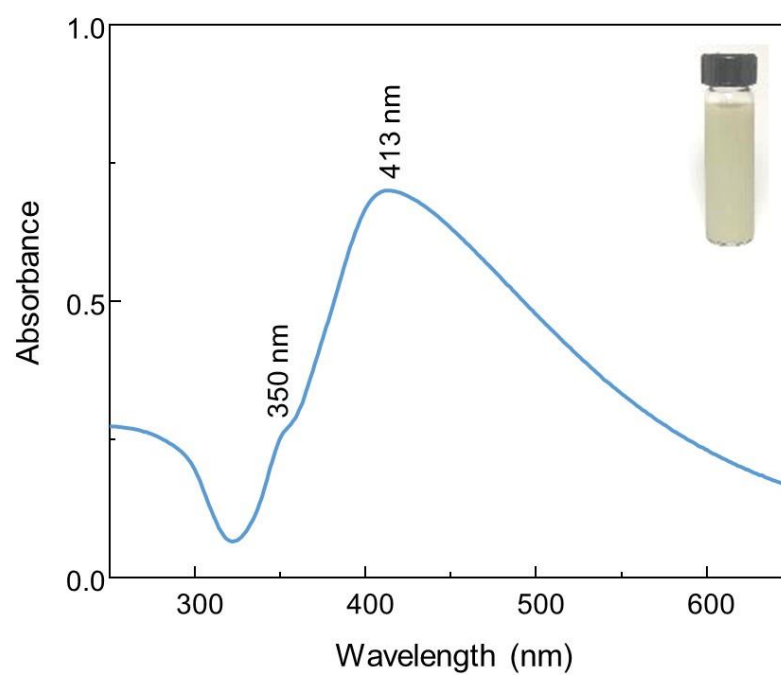
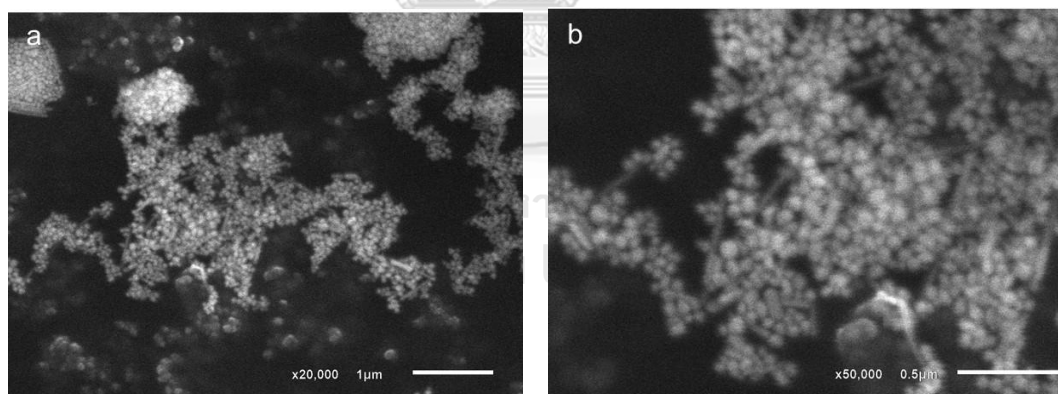


Figure 4.1 UV-visible spectrum of synthesized AgNPs colloid.



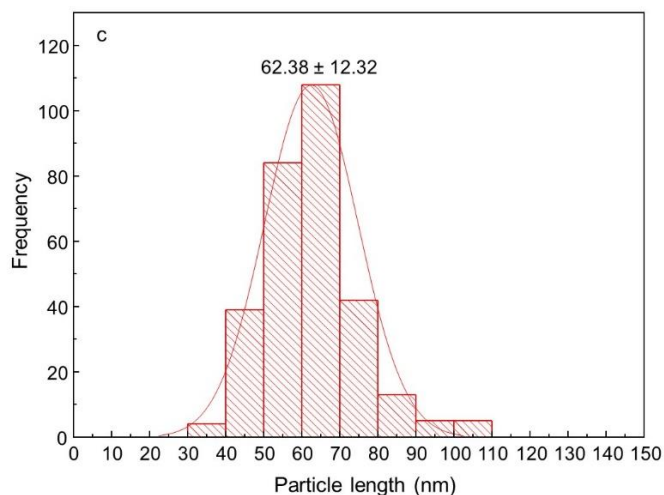


Figure 4.2 SEM image of AgNPs (a) x20.000, (b) x50.000, and (c) particle size of AgNPs.

4.2 Spectroscopic studies of R6G and Hg²⁺

UV–Visible spectroscopy was carried out to obtain the absorbance spectra of aqueous compounds. The UV-Visible spectra of Hg²⁺ and R6G are shown in Figure 4.3 and Figure 4.4, respectively. Since Hg²⁺ is colorless, it does not absorb in the visible region of the spectrum. However, there is a weak absorption in the UV region with a maximum at ~200 nm, which is characteristic of Hg²⁺ with nearly zero absorbance intensity.[84] Furthermore, R6G, a cationic dye, has a strong UV–visible absorption at 530 nm in water. This band is responsible for color originated from the aromatic rings connected by amino groups.[85]

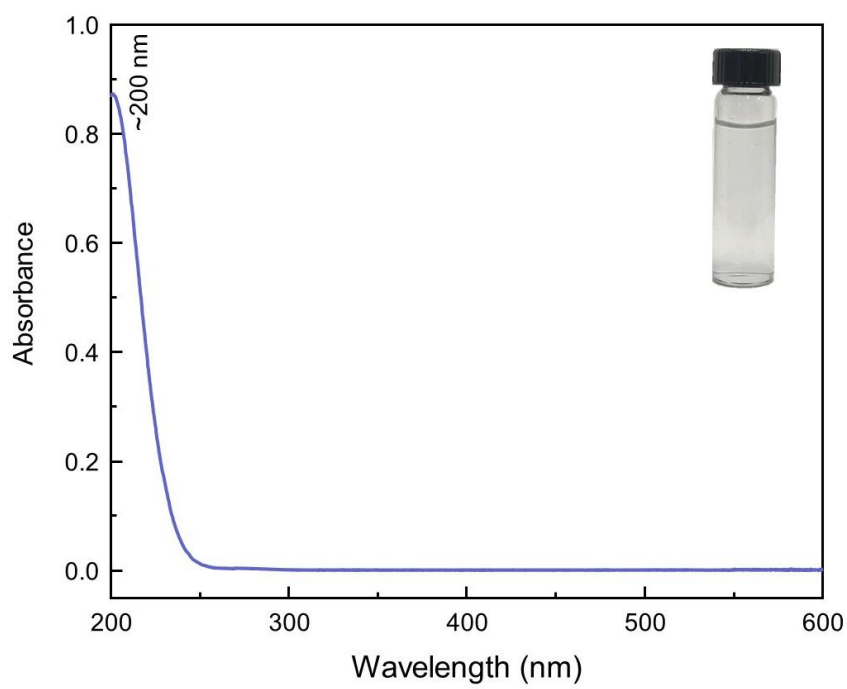


Figure 4.3 UV-visible spectrum of Hg^{2+} .

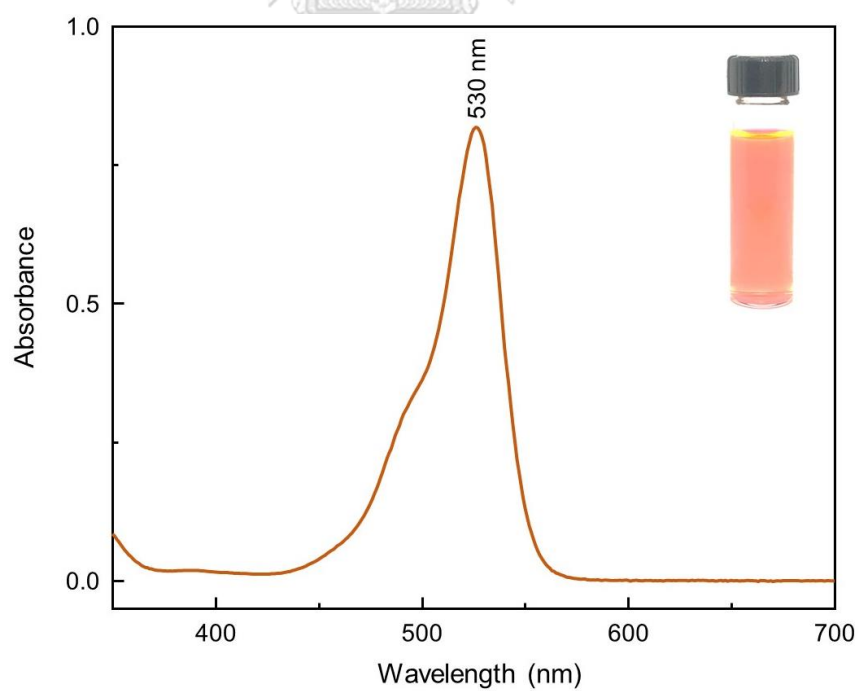


Figure 4.4 UV-visible spectrum of R6G.

4.3 Optical properties of the CQDs

The color of as-prepared CQDs was brownish, which exhibited the bright blue fluorescence under UV lamp with excitation of 360 nm (inset of Figure 4.5). The UV-visible spectrum of CQDs in Figure 4.5 shows a broad absorption band center at 346 nm attributes to $n\text{-}\pi^*$ transition of C=O bond. The broad absorption originated from the HOMO \rightarrow LUMO transition in surface fluorophore.[57, 86, 87] While the shoulder peak at 242 nm corresponds to $\pi\text{-}\pi^*$ transition of aromatic C=C bond within the carbogenic core of CQDs.[88, 89]

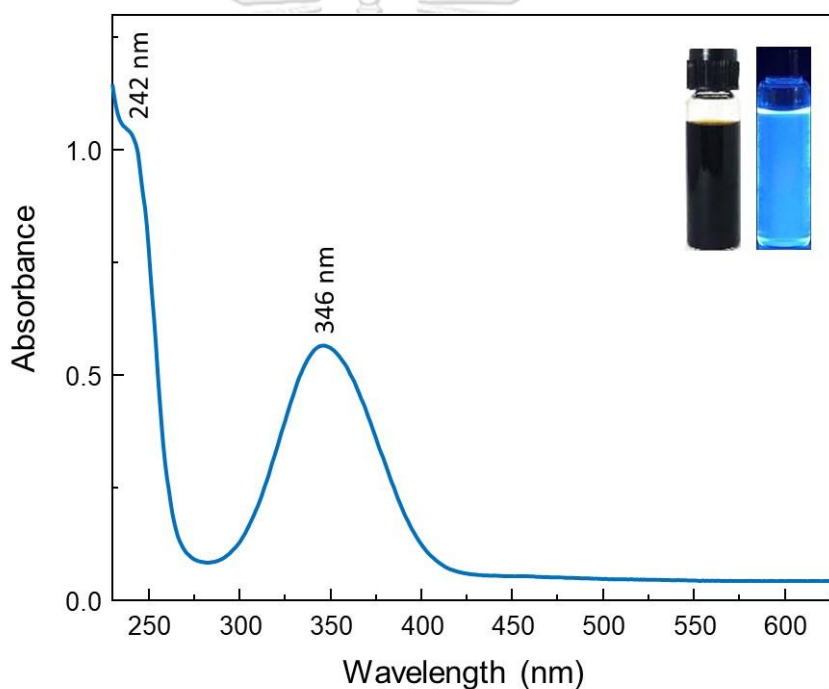


Figure 4.5 UV-visible spectrum of synthesized CQDs.

Figure 4.6 presents that the as-prepared CQDs exhibit strong fluorescence emission at 450 nm under a 346-nm excitation wavelength. Also, it reveals that the addition of Hg^{2+} significantly quenched the strong fluorescence emission of CQDs. The sensing principle for fluorescence quenching of CQDs by Hg^{2+} is due to the

facilitation of electron/hole recombination annihilation *via* an effective electron or energy transfer happening during the fluorescence quenching progress. These results indicate the special coordination interaction between Hg^{2+} ions and carboxylic groups of CQDs contribute to the quenching progress. Commonly, CQDs were used as electron donors to produce excited electrons after being irradiated by excitation light. Then, the excited electrons were transferred from CQDs to Hg^{2+} as the receptors, causing the fluorescence quenching of CQDs.[90-92]

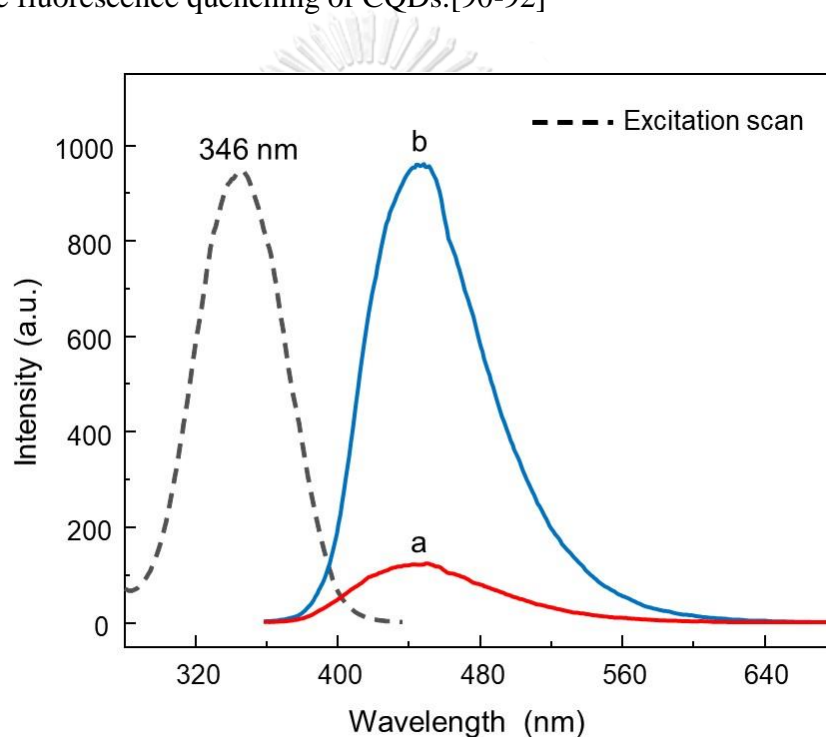


Figure 4.6 Fluorescence spectra of CQDs by using 346 nm excitation wavelength in the (a) presence and (b) absence of Hg^{2+} ($[\text{Hg}^{2+}] = 100 \text{ mg/L}$ in sample).

4.4 Raman spectra of AgNPs, CQDs, and CQDs in the presence of Hg^{2+}

This study investigated the viability of SERS as a method for the detection of Hg^{2+} . Raman spectra of AgNPs, CQDs, and CQDs in the presence of Hg^{2+} are shown in Figure 4.7. The only spectrum of AgNPs shows some peaks of citrate, which is a

stabilizer of AgNPs. While there is no peak observed for CQDs with and without Hg^{2+} , only the baseline shift can be detected due to the fluorescence of CQDs, in which the addition of Hg^{2+} decreases the intensity of the fluorescence signal. To some extent, SERS phenomena were affected by plasmon couplings and energy transfer processes involving metal or semiconducting substances. The fabrication of AgNPs conducted SERS-active spectra and the other nanostructures reproduce charge-transfer processes giving to more evident SERS signals.[93-95] This measurement proves that the coupling between AgNPs, R6G, CQDs, and Hg^{2+} , producing the SERS active spectrum for Hg^{2+} detection is necessary.

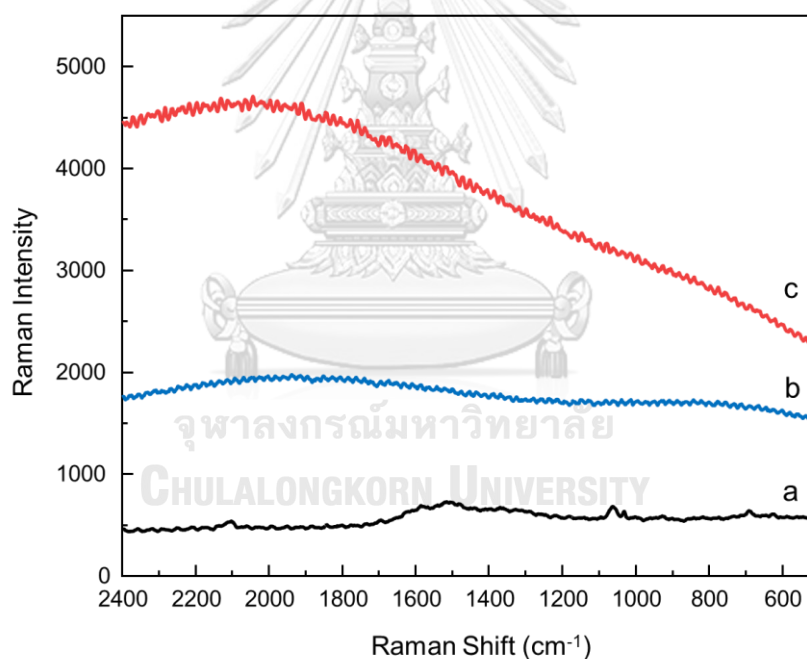


Figure 4.7 Raman spectra of (a) AgNPs, (b) CQDs, and (c) CQDs in the presence of Hg^{2+} (100 ng/L).

4.5 SERS detection of Hg^{2+} using AgNPs

Figure 4.8 shows Raman spectra collected from a drop of AgNPs, a drop of AgNPs with 100 ng/L Hg^{2+} , a dried film of AgNPs, and a dried film of AgNPs with

100 ng/L Hg^{2+} . No significant peak can be observed from a drops of AgNPs and a drops of AgNPs with Hg^{2+} . However, characteristic peaks of citrate can be observed from a dried film of AgNPs, and a dried film of AgNPs with Hg^{2+} . Table 4.1 shows the characteristic of citrate-covered AgNPs in SERS measurement. It is because silver nanoparticles of different sizes can be easily synthesized by the reduction of silver nitrate with trisodium citrate.[78] This chemical preparation process results in the formation of AgNPs with their surface covered by a molecular negatively charged citrate species, which have been widely used to detect positively charged analytes as well as some negatively charged ions.[96] Furthermore, Hg^{2+} could not be sensed optically because there was no significant appearance of Hg^{2+} peaks.

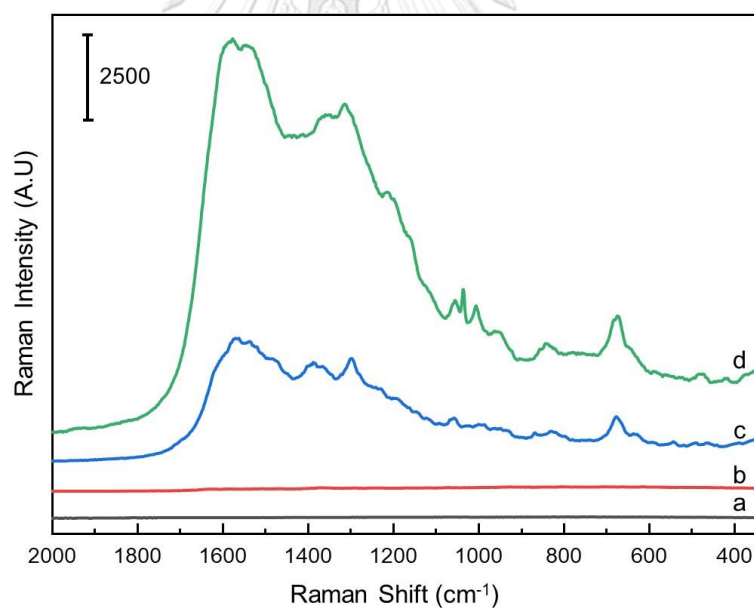


Figure 4.8 Raman spectra of (a) AgNPs, (b) AgNPs with Hg^{2+} ($[\text{Hg}^{2+}] = 100 \text{ ng/L}$), (c) dried AgNPs, and (d) dried AgNPs with Hg^{2+} ($[\text{Hg}^{2+}] = 100 \text{ ng/L}$).

The spectra in Figure 4.8 suggests that the presence of other molecules providing a second source of signal enhancement for Hg^{2+} detection is needed. The

results clearly represent the importance of determining the composition and surface chemistry of AgNPs to produce reproducibility in SERS signal. In this work, we have analyzed R6G adsorption on citrate-covered AgNPs by SERS. In particular, the interactions between citrate-covered AgNPs and R6G causes charge transfer within complexes, leading to a change in polarizability as well as in Raman response of the system. The interactions between AgNPs and R6G induces large SERS enhancement that can be shown in Figure 4.9.

Table 4.1 Band assignments of citrate

peak position (cm ⁻¹)		band assignments
trisodium-citrate (785-nm excitation laser)[97]	this work (532-nm excitation laser)	
1601	1566	νCO^{2-} asym
1388	1385	νCO^{2-} sym + $\delta_{\text{CH}_2} + \omega_{\text{CH}_2}$
1288	1296	$\nu\text{C-O} + \delta_{\text{OH}}$
1063	1058	νCC , sym
955	986	νCCO , trans
895	865	$\nu\text{C-COOH} + \nu\text{CC}(\text{trans-trans})$
843	833	$\nu\text{C}_4\text{O}$, sym + ρ_{CH_2}
675	675	δ_{COO}
622	631	ω_{COO^-}
595	595	$\delta_{\text{CCO}} + \tau_{\text{CCCC}}$
545	544	$\gamma_{\text{CCO}} + \delta_{\text{CCO}}$

Table 4.2 Basic types of vibrations and their description with Greek symbols [98]

Symbol	Description	
ν	stretching	sym = symmetric asym = antisymmetric
δ	bending	
ρ	rocking	
ω	wagging	
τ	twisting	

4.6 Optimization of R6G concentration in SERS measurement

In this study, R6G dye, which is commonly used in SERS investigations because of its immense intensity enhancement and absorbability onto nanoparticles, is used as a probe molecule to give Raman signals, which indirectly indicate whether there is Hg^{2+} in the system.[99, 100] From Figure 4.9a shows SERS spectra obtained from R6G absorbed on AgNPs, which were coupled with CQDs and Hg^{2+} (100 ng/L). The concentrations of R6G are ranging from 1.0×10^{-4} , 1.0×10^{-5} , 1.0×10^{-6} , 1.0×10^{-7} , and 1.0×10^{-8} M. As displayed in Figure 4.9a, the characteristic of R6G Raman peaks are not visible for the concentrations of 1.0×10^{-4} to 1.0×10^{-6} M due to its high fluorescence background. The Raman peak intensity gradually decreases with a decrease in R6G concentration from 1.0×10^{-7} M to 1.0×10^{-8} M. The characteristic peaks of R6G were clearly recognized at the R6G concentration of 1.0×10^{-7} M as the highest peak intensity. Table 4.3 shows band assignments of R6G absorbed on AgNPs. Therefore, 1.0×10^{-7} M R6G was used for further SERS measurements.

Figure 4.9b shows SERS spectra obtained from R6G adsorbed on AgNPs, which were coupled with CQDs in the absence of Hg^{2+} . The clear characteristic Raman peaks of R6G cannot be observed, even in 1.0×10^{-7} M R6G, due to the fluorescence background from CQDs, causing Raman peaks of R6G to be buried by the fluorescence background of CQDs. The quenching of CQDs fluorescence is conducted by Hg^{2+} , as shown in Figure 4.9a. Therefore, in this work, the intensity of R6G characteristic peaks in the presence of Hg^{2+} can be used to determine the concentration of Hg^{2+} in samples by using SERS measurement.

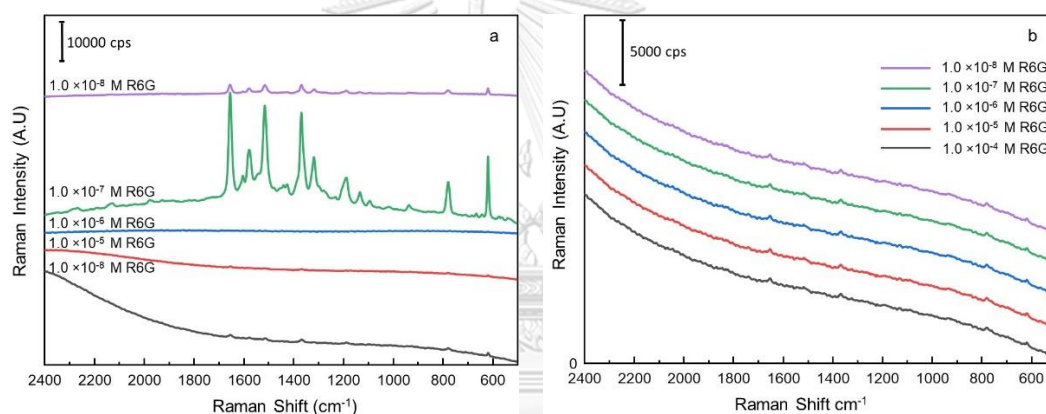


Figure 4.9 SERS spectra collected from R6G (10^{-4} M to 10^{-8} M) adsorbed on AgNPs, which were coupled with CQDs in the (a) presence and (b) absence of Hg^{2+} (100 ng/L).

Table 4.3 Band assignments of R6G Raman spectrum

peak position (cm ⁻¹)		band assignments
this work	reference[101]	
1651	1652	Aromatic C—C stretching
1577	1575	Aromatic C—C stretching
1510	1509	Aromatic C—C stretching
1367	1365	Aromatic C—C stretching
1316	1312	C—O—C stretching
1187	1187	Aromatic C-H bending
773	776	C—H out of plane bending
615	614	C—C—C ring in plane bending

4.7 SERS detection of Hg²⁺ using CQDs incorporated with Rhodamine 6G

Figure 4.10 clearly shows that the coupling between AgNPs, R6G 1.0×10^{-7} M, and CQDs enabled SERS detection for Hg²⁺. The measurement were performed with different concentrations of Hg²⁺ ranging from 0.100, 0.500, 1.00, 5.00, 10.0, 50.0, and 100 ng/L. The peak intensity of R6G was affected by the existence of CQDs fluorescence and Hg²⁺ concentration. R6G peaks can be overwhelmed by the strong fluorescence of CQDs, which the addition of Hg²⁺ can generate a strong SERS signal due to the quenching of CQDs fluorescence. The intensity of R6G in the SERS spectra obtained at 532-nm excitations is significantly high at 100 ng/L of Hg²⁺ concentration, showing that the R6G peak is not overwhelmed by CQDs fluorescence and more visible. A decrease in the concentration of Hg²⁺ leads to a decrease in the

intensity of SERS signal. In Figure 4.10, SERS spectra demonstrate a clear correlation between the intensity of SERS signal and Hg^{2+} concentration.

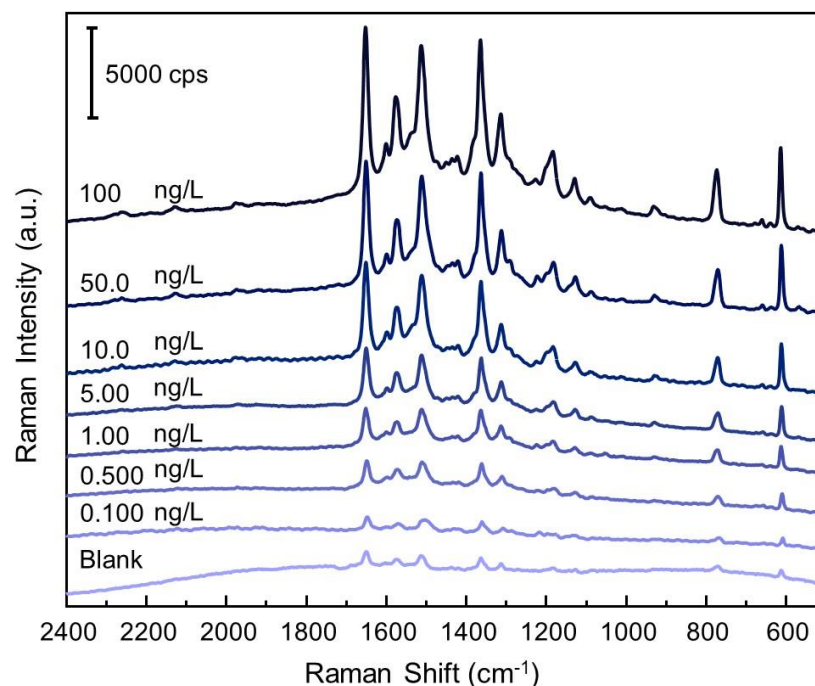


Figure 4.10 SERS spectra of R6G incorporated with CQDs and Hg^{2+} at different Hg^{2+} concentrations.

Figure 4.11 displays a plot of R6G peak intensity at 615 cm^{-1} (I_{615}) as a function of Hg^{2+} concentration. A strong and sharp Raman peak at 615 cm^{-1} corresponds to C—C—C ring in-plane bending. This peak intensity is used as an indicator of Hg^{2+} concentrations. The concentrations of Hg^{2+} were varied as 0.100, 0.500, 1.00, 5.00, 10.0, 50.0, and 100 ng/L. As the concentration of Hg^{2+} is decreased, the peak intensity at 615 cm^{-1} decreases. Even at the low Hg^{2+} concentration of 0.100 ng/L, the peak intensity at 615 cm^{-1} is still observed and can be differentiated from the blank.

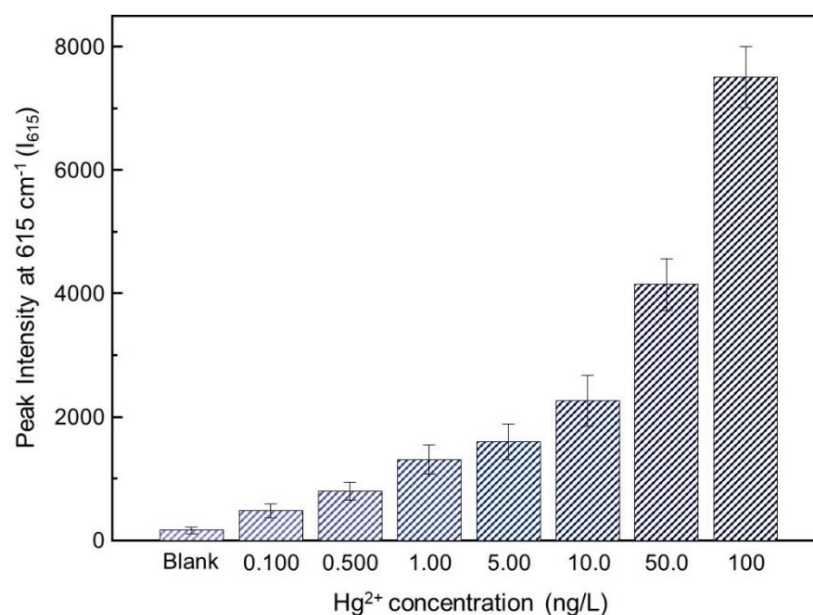


Figure 4.11 Plot of I_{615} against Hg^{2+} concentration (0.100-100 ng/L).

To quantify Hg^{2+} by using our proposed technique, the peak intensity of R6G was linearly plotted against the concentration of Hg^{2+} . Figure 4.12 shows the linear fitting curve of R6G peak intensities at 615 cm^{-1} (I_{615}) versus Hg^{2+} concentrations ranging from 0.100, 0.200, 0.400, 0.500, 0.600, and 0.800 ng/L, which exhibited a good linear relationship with a correlative efficiency $R^2 = 0.963$, indicating excellent ability to quantitative SERS analysis by using the proposed SERS technique. Therefore, the limit of detection (LOD) of Hg^{2+} that can be determined was found to be at 0.190 ng/L.

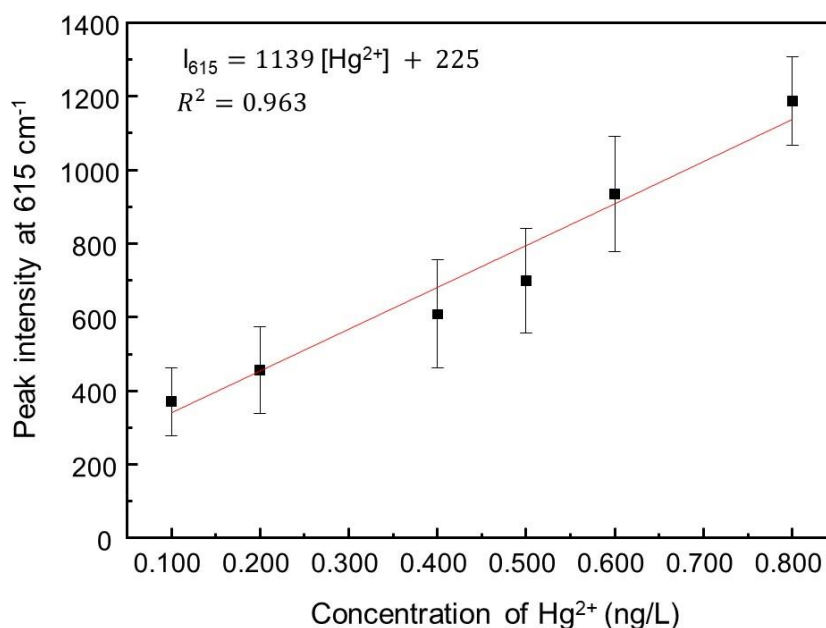


Figure 4.12 The correlation of Hg²⁺ concentration (0.100–0.800 ng/L) and peak intensity of R6G at 615 cm⁻¹.

4.8 Selectivity of Hg²⁺ detection

Selectivity is another critical parameter to evaluate the performance of the sensing system. Figure 4.13 depicts the SERS response of the system to various metal cations and their selectivity for Hg²⁺. The selectivity of CQDs against a more complex background containing Hg²⁺ and another interfering ion is evaluated. The investigation was conducted by measuring 1.00 ng/L of Hg²⁺ in the presence of 1% of various metal ions (Al³⁺, Ca²⁺, Cu²⁺, Cd²⁺, Co²⁺, Fe²⁺, Fe³⁺, K⁺, Mn²⁺, Ni²⁺, Pb²⁺, Sn²⁺, and Zn²⁺). As shown in Figure 4.13, most of the metal ions could not induce obvious changes in peak intensity at 615 cm⁻¹. The probe still exhibits good performance in the presence of other interfering ions. This may be ascribed to the fact that Hg²⁺ has a stronger affinity towards the rich carboxylic group on the surface of CQDs.[102] The results approve the efficiency of this system to detect Hg²⁺.

However, this method needs to be implemented in the real samples for further applications.

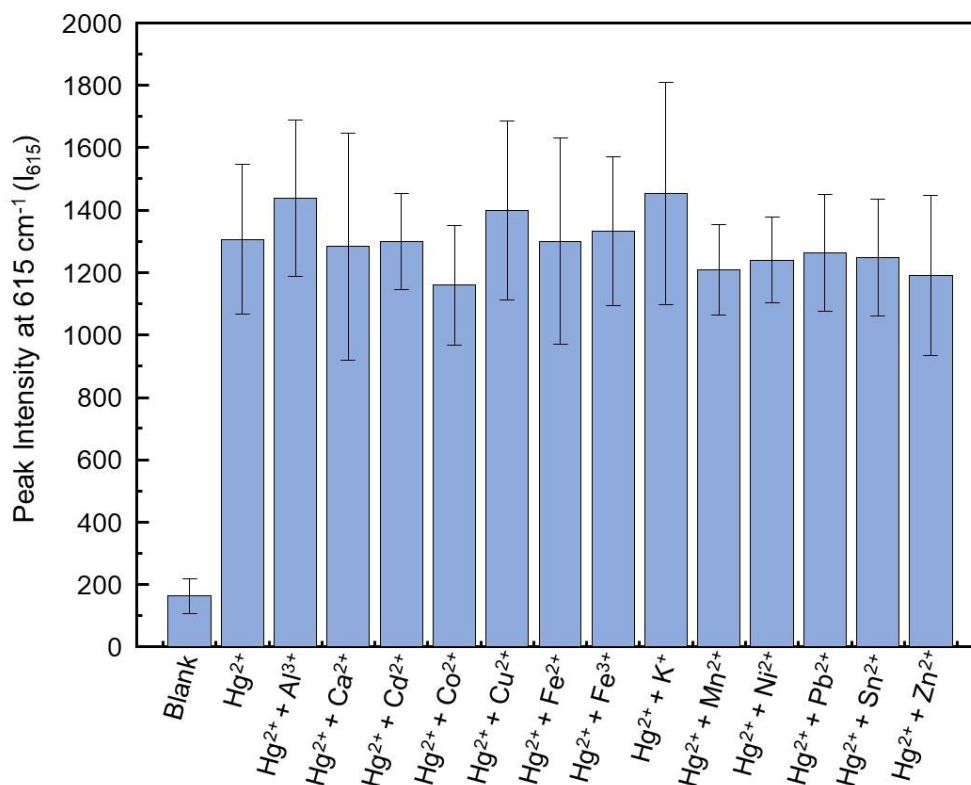


Figure 4.13 I₆₁₅ measured from samples containing Hg²⁺ and interfering metal ions. The concentration of Hg²⁺ is 1.00 ng/L in the presence of 1% of another interfering metal ions.

4.9 Determination of Hg²⁺ in a mineral drinking water sample

The application of this technique was demonstrated by detecting Hg²⁺ in real water samples. Apart from the elemental mercury, the main mercury species in water are Hg²⁺ and mercury-organic species, particularly methylmercury. It has strong bioaccumulation in living organisms. Its presence in the water determined the relative concentration of mercury in an organism. Therefore, the mineral drinking water sample was considered as a real water sample. The mineral drinking water spiked

with Hg^{2+} was used to imitate the Hg^{2+} contaminated water for testing this sensor practicability. The addition of Hg^{2+} concentration in mineral water was ranging from 0.100–100 ng/L. The SERS spectra in Figure 4.14 show that the containing Hg^{2+} in mineral drinking water resulted in the changes of SERS signal intensity as the different concentration of Hg^{2+} was added. The SERS signal intensity decreases as the concentration of Hg^{2+} decreases. By plotting I_{615} against Hg^{2+} concentration, as shown in Figure 4.15. It shows that higher Hg^{2+} concentrations could quench the fluorescence of CQDs effectively, resulting in the enhancement of the peak intensity and more apparent spectra.

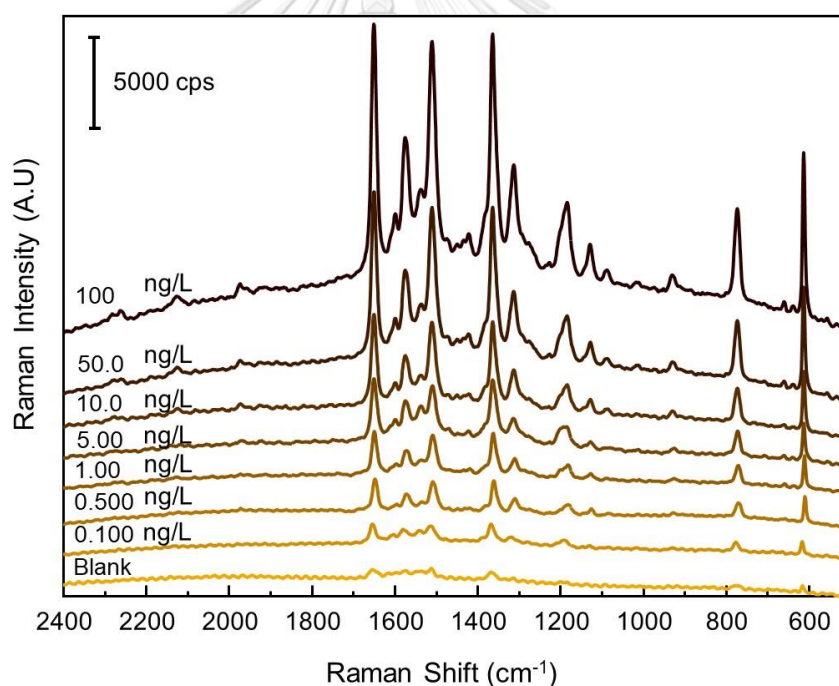


Figure 4.14 SERS spectra of R6G incorporated with CQDs and Hg^{2+} at different Hg^{2+} concentrations (0.100-100 ng/L) in mineral drinking water.

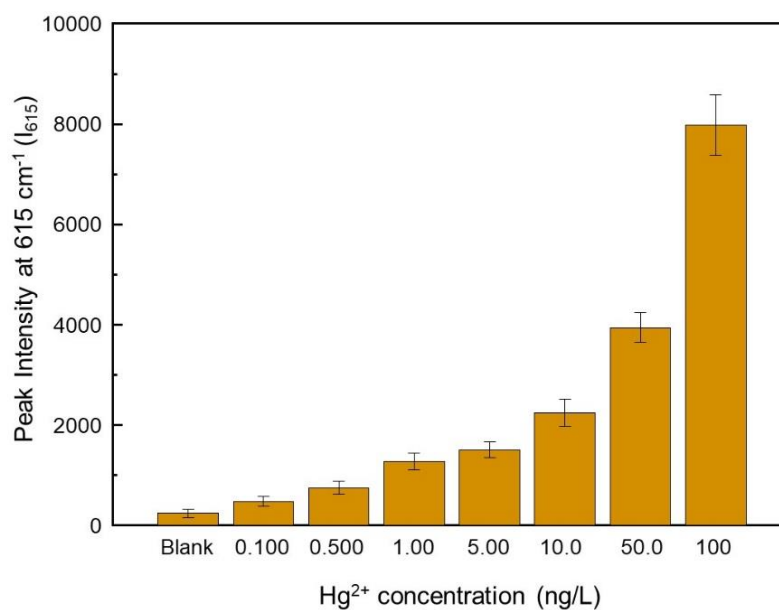


Figure 4.15 Plot of peak intensity at 615 cm⁻¹ (I₆₁₅) against Hg²⁺ concentration (0.1-100 ng/L) in mineral drinking water.

Figure 4.16 depicts the linear fitting results for I₆₁₅ versus Hg²⁺ concentration in a mineral drinking water sample ranging from 0.100, 0.200, 0.400, 0.500, 0.600, and 0.800 ng/L, which yielded $R^2 = 0.935$ value. The limit of detection (LOD) of Hg²⁺ in a mineral drinking water sample was found to be at 0.194 ng/L. The LOD of Hg²⁺ in mineral drinking water is similar to the LOD of Hg²⁺ in deionized water (LOD = 0.190 ng/L). The experimental results reveal that this SERS technique is potentially applicable for detecting Hg²⁺ in real water samples.

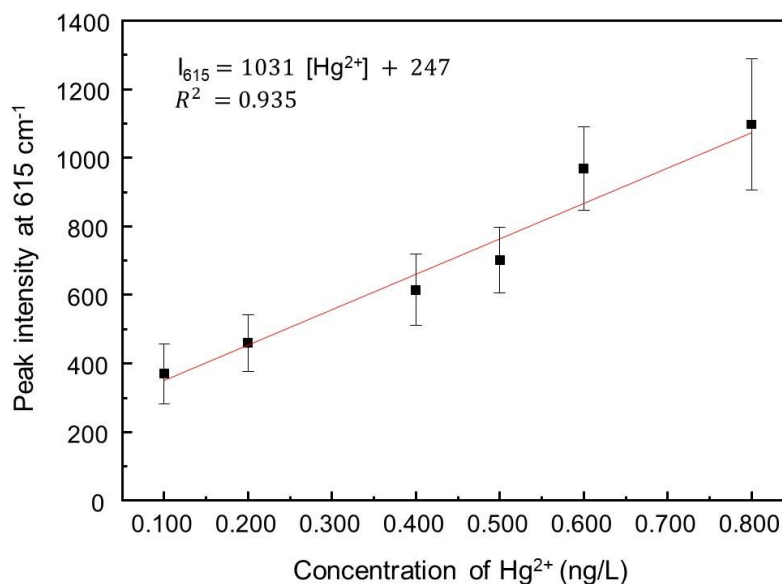


Figure 4.16 The correlation of Hg²⁺ concentration (0.100–0.800 ng/L) and peak intensity of R6G at 615 cm⁻¹ in mineral drinking water.

4.10 Validation for Hg²⁺ determination method

The validation process for this proposed method has been investigated in order to confirm a good accuracy. The technique which is appropriated for the determination of Hg²⁺ in water sample is inductively coupled plasma optical emission spectrometry (ICP-OES). The closeness between the true concentration value of Hg²⁺ in sample by ICP-OES and the concentration value of Hg²⁺ obtained by our method was used to validate our method. The Hg²⁺ was spiked into a mineral drinking water. Table 4.4 shows the ICP-OES results of Hg²⁺ concentration that was spiked in a mineral drinking water sample. From Table 4.4, the spiked Hg²⁺ concentration measured by our method was 0.1043 mg/L, while the concentration measured by the proposed method was 0.101 ± 0.014 ng/L. It shows that the Hg²⁺ concentrations from ICP-OES results and SERS measurements by our method are insignificantly different.

Therefore, we can prove that our method is validated and can be used for Hg^{2+} detection.

Table 4.4 Validation method for determination of Hg^{2+}

parameters	Concentration of Hg^{2+} by ICP-OES method (mg/L)	Concentration of Hg^{2+} by proposed method (mg/L)
Hg^{2+} in mineral drinking water	0.1043 ± 0.0086	0.101 ± 0.014



CHAPTER 5

CONCLUSIONS

A new SERS method for Hg^{2+} detection is proposed based on the drawback of fluorescence in SERS. In this work, we have performed the coupling set up of AgNPs, R6G, and CQDs for sensitive, selective, and convenient analysis of Hg^{2+} . AgNPs have an important role in creating hotspot for enhancing the SERS signal. At the same time, R6G was used as an indicator for Hg^{2+} by measuring the changes of R6G intensity. Fluorescence of CQDs is quenched as an addition of Hg^{2+} , producing strong signal of R6G. As the concentration of Hg^{2+} decreased, the R6G signal is decreased due to an intense fluorescence background of CQDs overwhelmed R6G signal. The Raman intensity at 615 cm^{-1} from SERS spectra of R6G was plotted against the concentrations of Hg^{2+} . The peak refers to the C—C—C ring in-plane bending vibration as the characteristic bands of R6G. Based on the results, the linear calibration curve of Raman intensity with $R^2 = 0.963$ was accomplished in ranging from 0.100, 0.200, 0.400, 0.500, 0.600, and 0.800 ng/L with the limit of detection (LOD) of 0.190 ng/L. The selectivity of our developed method was also investigated by adding interfering metal ions. The addition of interfering metal ions (Al^{3+} , Ca^{2+} , Cu^{2+} , Cd^{2+} , Co^{2+} , Fe^{2+} , Fe^{3+} , K^+ , Mn^{2+} , Ni^{2+} , Pb^{2+} , Sn^{2+} , and Zn^{2+}) showed that our developed technique still presents good performance in the presence of other interfering ions. Moreover, the practical application of Hg^{2+} detection in a real water sample using our developed technique was applicable in a mineral drinking water. Raman intensity with $R^2 = 0.935$ was achieved as the linear calibration curve in mineral drinking water with Hg^{2+} in the concentration range of 0.100, 0.200, 0.400,

0.500, 0.600, and 0.800 ng/L and the limit of detection (LOD) that can be determined as 0.194 ng/L. An inductively coupled plasma optical emission spectrometry (ICP-OES) was performed to determine Hg^{2+} in sample and validate our method. The ICP-OES technique measured the Hg^{2+} concentration in a mineral drinking water was 0.1043 ± 0.0086 mg/L. Compared with our method, the concentration of Hg^{2+} that can be found in mineral drinking water was 0.101 ± 0.014 . It shows that our method is validated due to the similar results between measuring by ICP-OES and our method.

From the results, SERS technique using the fluorescence-quenched CQDs to detect Hg^{2+} ranging from 0.100, 0.200, 0.400, 0.500, 0.600, 0.800, 1.00, 5.00, 10.0, 50.0, and 100 ng/L has a simple sample preparation procedure compared to the other techniques. It also provides a sensitive, selective, and convenient analysis with low-cost and high-intensity SERS signal.

REFERENCES

- [1] Mahadevan-Jansen, A.; Richards-Kortum, R. R. Raman Spectroscopy for The detection of Cancers and Precancers. *Journal of Biomedical Optics* **1996**, *1*(1), 31-71.
- [2] Koo, T. W.; Berger, A. J.; Itzkan, I.; Horowitz, G.; Feld, M. S., Reagentless Blood Analysis by Near-Infrared Raman Spectroscopy. *Diabetes Technology & Therapeutics* **1999**, *1*(2) 153-157.
- [3] Shih, W. C.; Bechtel, K. L.; Feld, M. S., Intrinsic Raman Spectroscopy for Quantitative Biological Spectroscopy Part I: Theory and Simulations. *Optics Express* **2008**, *16*(17),12726-12736.
- [4] Smith, R.; Wright, K. L.; Ashton, L., Raman Spectroscopy: An Evolving Technique for Live Cell Studies. *Journal of Analyst* **2016**, *141*(12), 3590-3600.
- [5] Smith, E.; Dent, G., Modern Raman Spectroscopy: A Practical Approach. **2005**, 129-150.
- [6] Friedman, J. M.; Hochstrasser, R. M., The Use of Fluorescence Quenchers in Resonance Raman Spectroscopy. *Journal of Chemical Physics Letter* **1975**, *33*(2), 225-227.
- [7] Wieczorek-Dąbrowska, M.; Tomza-Marciniak, A.; Pilarczyk, B.; Balicka-Ramisz, A., Roe and Red Deer as Bioindicators of Heavy Metals Contamination in North-Western Poland. *Journal of Chemistry and Ecology* **2013**, *29*(2), 100-110.
- [8] Renzoni, A.; Zino, F.; Franchi, E., Mercury Levels Along The Food Chain and Risk for Exposed Populations. *Journal of Environmental Research* **1998**, *77*(2), 68-72.
- [9] Malm, O., Gold Mining as A Source of Mercury Exposure in The Brazilian Amazon. *Journal of Environmental Research* **1998**, *77*(2), 73-78.
- [10] Santé, O. M. D. L.; Zdrowia, S. O.; Organization, W. H.; Staff, W. H. O., *Guidelines for Drinking-Water Quality Vol. 1*, World Health Organization **2004**.
- [11] Tchounwou, P. B.; Ayensu, W. K.; Ninashvili, N.; Sutton, D., Environmental Exposure to Mercury and Its Toxicopathologic Implications for Public Health, *Journal of Environmental Toxicology: An International Journal* **2003**, *18*(3), 149-175.
- [12] Clifton II, J. C., Mercury Exposure and Public Health. *Journal of Pediatric Clinics of North America* **2007**, *54*(2), 237.
- [13] Mao, Y.; Liu, G.; Meichel, G.; Cai, Y.; Jiang, G., Simultaneous Speciation of Methylmercury and Monoethylmercury by Aqueous Phenylation and Purge-and-Trap Preconcentration Followed by Atomic Spectrometry Detection. *Journal of Analytical Chemistry* **2008**, *80*(18), 7163-7168.
- [14] Hippler, J.; Hoppe, H.; Mosel, F.; Rettenmeier, A.; Hirner, A., Comparative Determination of Methyl Mercury in Whole Blood Samples Using GC-ICP-MS and GC-MS Techniques. *Journal of Chromatography* **2009**, *877*(24), 2465-2470.
- [15] Lemos, V.A; Dos Santos, L.O., A New Method for Preconcentration and Determination of Mercury in Fish, Shellfish and Saliva by Cold Vapour Atomic Absorption Spectrometry. *Journal of Food Chemistry* **2014**, *149*, 203-207.
- [16] Lim, J.W.; Kim, T.Y.; Choi, S. W.; Woo, M. A., 3D-Printed Rolling Circle Amplification Chip for On-Site Colorimetric Detection of Inorganic Mercury in Drinking Water. *Journal of Food Chemistry* **2019**, *300*, 125177.
- [17] Lu, F.; Zhang, S.; Gao, H.; Jia, H.; Zheng, L., Protein-Decorated Reduced Oxide Graphene Composite and Its Application to SERS. *Journal of ACS Applied Materials & Interfaces* **2012**, *4*(6), 3278-3284.
- [18] Cerf, A.; Molnár, G.; Vieu, C., Novel Approach for The Assembly of Highly Efficient SERS Substrates. *Journal of ACS Applied Materials & Interfaces* **2009**, *1*(11), 2544-2550.
- [19] Li, X.; Hu, H.; Li, D.; Shen, Z.; Xiong, Q.; Li, S.; Fan, H. J., Ordered Array of Gold

- Semishells on TiO₂ Spheres: An Ultrasensitive and Recyclable SERS Substrate. *Journal of ACS Applied Materials & Interfaces* **2012**, 4(4), 2180-2185.
- [20] Li, J.; Chen, L.; Lou, T.; Wang, Y., Highly Sensitive SERS Detection of As³⁺ Ions in Aqueous Media Using Glutathione Functionalized Silver Nanoparticles. *Journal of ACS Applied Materials & Interfaces* **2011**, 3(10), 3936-3941.
- [21] Ding, X.; Kong, L.; Wang, J.; Fang, F.; Li, D.; Liu, J., Highly Sensitive SERS Detection of Hg²⁺ Ions in Aqueous Media Using Gold Nanoparticles/Graphene Heterojunctions. *Journal of ACS Applied Materials & Interfaces* **2013**, 5(15), 7072-7078.
- [22] Song, C.; Yang, B.; Zhu, Y.; Yang, Y.; Wang, L., Ultrasensitive Silver Nanorods Array SERS Sensor for Mercury Ions. *Journal of Biosensors and Bioelectronics* **2017**, 87, 59-65.
- [23] Zeng, Y.; Wang, L.; Zeng, L.; Shen, A.; Hu, J., A Label-free SERS Probe for Highly Sensitive Detection of Hg²⁺ Based on Functionalized Au@ Ag Nanoparticles. *Journal of Talanta* **2017**, 162, 374-379.
- [24] Guselnikova, O.; Svorcik, V.; Lyutakov, O.; Chehimi, M. M.; Postnikov, P. S., Preparation of Selective and Reproducible SERS Sensors of Hg²⁺ Ions via a Sunlight-Induced Thiol–Yne Reaction on Gold Gratings. *Journal of Sensors* **2019**, 19(9), 2110.
- [25] Zhao, Y.; Yamaguchi, Y.; Ni, Y.; Li, M.; Dou, X., A SERS-Based Capillary Sensor for The Detection of Mercury Ions in Environmental Water. *Journal of Spectrochimica Acta Part A: Molecular and Biomolecular Spectroscopy* **2020**, 118193.
- [26] Hao, B.; Bu, X.; Wu, J.; Ding, Y.; Zhang, L.; Zhao, B.; Tian, Y., Determination of Hg²⁺ in Water Based on Acriflavine Functionalized AgNPs by SERS. *Journal of Microchemical* **2020**, 155, 104736.
- [27] Zhu, X.; Xu, T.; Lin, Q.; Duan, Y., Technical Development of Raman Spectroscopy: From Instrumental to Advanced Combined Technologies. *Journal of Applied Spectroscopy* **2014**, 49(1), 64-82.
- [28] Lewis, I. R.; Edwards, H., *Handbook of Raman spectroscopy: from the research laboratory to the process line*, CRC press **2001**.
- [29] Popp, J.; Mayerhöfer, T., *Micro-Raman Spectroscopy: Theory and Application*. Walter de Gruyter GmbH & Co KG **2020**.
- [30] Brewer, P.G.; Malby, G.; Pasteris, J. D.; White, S. N.; Peltzer, E. T.; Wopenka, B.; Brown, M. O., Development of A Laser Raman Spectrometer for Deep-Ocean Science. *Deep sea Research Part I: Oceanographic Research Papers* **2004**, 51(5), 739-753.
- [31] Dunk, R. M.; Peltzer, E. T.; Walz, P. M.; Brewer, P. G., Seeing A Deep Ocean CO₂ Enrichment Experiment in A New Light: Laser Raman Detection of Dissolved CO₂ in Seawater. *Journal of Environmental Science & Technology* **2005**, 39(24), 9630-9636.
- [32] Li, H.; Zhai, J.; Tian, J.; Luo, Y.; Sun, X., Carbon Nanoparticle for Highly Sensitive and Selective Fluorescent Detection of Mercury (II) Ion in Aqueous Solution. *Journal of Biosensors and Bioelectronics* **2011**, 26(12), 4656-4660.
- [33] Haynes, C. L.; Yonzon, C. R.; Zhang, X.; Van Duyne, R. P., Surface-Enhanced Raman Sensors: Early History and The Development of Sensors for Quantitative Biowarfare Agent and Glucose Detection. *Journal of Raman Spectroscopy: An International Journal for Original Work in All Aspects of Raman Spectroscopy, Including Higher Order Processes, and also Brillouin and Rayleigh Scattering* **2005**, 36(6-7), 471-484.
- [34] Kneipp, K.; Moskovits, M.; Kneipp, H., Surface-Enhanced Raman Scattering. *Journal of Physics Today* **2007**, 60(11), 40.
- [35] Valley, N.; Greeneltch, N.; Van Duyne, R. P.; Schatz, G. C., A Look At The Origin and Magnitude of The Chemical Contribution to The Enhancement Mechanism of Surface-Enhanced Raman Spectroscopy (SERS): Theory and Experiment. *Journal of Physical Chemistry Letters* **2013**, 4(16), 2599-2604.
- [36] Tong, L.; Zhu, T.; Liu, Z.; Approaching The Electromagnetic Mechanism of Surface-Enhanced Raman Scattering: From Self-Assembled Arrays to Individual Gold

- Nanoparticles. *Journal of Chemical Society Reviews* 2011, 40(3), 1296-1304.
- [37] Campion, A.; Kambhampati, P., Surface-enhanced Raman scattering. *Journal of Chemical Society Reviews* **1998**, 27(4), 241-250.
- [38] Etchegoin, P. G., Quo Vadis Surface-Enhanced Raman Scattering **2009**.
- [39] Kneipp, K., Single Molecule Detection Using Surface-Enhanced Raman Scattering (SERS). *Journal Physical Review Letters* 1997, 78(9), 1667.
- [40] Willets, K. A; Van Duyne, R. P., Localized Surface Plasmon Resonance Spectroscopy and Sensing. *Journal of Annual Review of Physical Chemistry* **2007**, 58, 267-297.
- [41] Liu, D.; Wu, W.; Qiu, Y.; Lu, J.; Yang, S., Chemical Conjugation of Fullerene C60 to CdSe Nanocrystals via Dithiocarbamate Ligands. *The Journal of Physical Chemistry C* **2007**, 111(48), 17713-17719.
- [42] Albrecht, M. G.; Creighton, J. A., Anomalously Intense Raman Spectra of Pyridine At A Silver Electrode. *Journal of The American Chemical Society* **1977**, 99(15), 5215-5217.
- [43] Langer, J.; Jimenez de Aberasturi, D.; Aizpurua, J.; Alvarez-Puebla, R. A.; Baumberg, J. J.; Choo, J., Present and Future of Surface-Enhanced Raman Scattering. *Journal of ACS Nano* **2019**, 14(1), 28-117.
- [44] Nam, J. M.; Oh, J. W.; Lee, H.; Suh, Y. D., Plasmonic Nanogap-Enhanced Raman Scattering With Nanoparticles. *Journal of Accounts of Chemical Research* **2016**, 49(12), 2746-2755.
- [45] Hoang, L. T.; Van Pham, H.; Nguyen, M. T. T., Investigation of The Factors Influencing The Surface-Enhanced Raman Scattering Activity of Silver Nanoparticles. *Journal of Electronic Materials* **2020**, 49(3), 1864-1871.
- [46] Mosier-Boss, P. A., Review of SERS Substrates for Chemical Sensing. *Journal of Nanomaterials* **2017**, 7(6), 142.
- [47] Pilot, R.; Signorini, R.; Durante, C.; Orian, L.; Bhamidipati, M.; Fabris, L., A Review on Surface-Enhanced Raman Scattering. *Journal of Biosensor* **2019**, 9(2), 57.
- [48] Otto, A., Charge Transfer in First Layer Enhanced Raman Scattering and Surface Resistance. *Q. Journal of Physical Review* **2017**, 3, 1-14.
- [49] Fisher, J. F.; World Health Organization, *Elemental mercury and inorganic mercury compounds: human health aspects*. World Health Organization, **2003**.
- [50] World Health Organization, *Methylmercury*. World Health Organization. **1990**.
- [51] Rezaee, A.; Derayat, J.; Mortazavi, S.; Yamini, Y.; Jafarzadeh, M., Removal of Mercury From Chlor-Alkali Industry Wastewater Using Acetobacter Xylinum Cellulose. *American Journal of Environmental Sciences* **2005**, 1(2), 102-105.
- [52] Tangahu, B.V.; Sheikh Abdullah, S. R.; Basri, H.; Idris, M.; Anuar, N.; Mukhlisin, M., A Review on Heavy Metals (As, Pb, and Hg) Uptake by Plants Through Phytoremediation. *International Journal of Chemical Engineering* **2011**.
- [53] Berlin, M.; Zalups, R.; Fowler, B., *Mercury. Handbook on The Toxicology of Metals*. Elsevier Inc. **2007**.
- [54] Wypych, G., *Functional Fillers: Chemical Composition, Morphology, Performance, Applications*. Elsevier. **2018**.
- [55] Bhunia, S. K.; Nandi, S.; Shikler, R.; Jelinek, R., Tuneable Light-Emitting Carbon-Dot/Polymer Flexible Films Prepared Through One-Pot Synthesis. *Journal of Nanoscale* **2016**, 8(6), 3400-3406.
- [56] Liu, M. L.; Chen, B. B.; Li, C. M.; Huang, C. Z., Carbon Dots: Synthesis, Formation Mechanism, Fluorescence Origin and Sensing Applications. *Journal of Green Chemistry* **2019**, 21(3), 449-471.
- [57] Zhu, S.; Meng, Q.; Wang, L.; Zhang, J.; Song, Y.; Jin, H.; Yang, B., Highly Photoluminescent Carbon Dots for Multicolor Patterning, Sensors, and Bioimaging. *Angewandte* **2013**, 125(14), 4045-4049.
- [58] Liang, Y.; Zhang, H.; Zhang, Y.; Chen, F., Simple Hydrothermal Preparation of Carbon

- Nanodots and Their Application in Colorimetric and Fluorimetric Detection of Mercury Ions. *Journal of Analytical Methods* **2015**, 7(18), 7540-7547.
- [59] Bhunia, S. K.; Pradhan, N.; Jana, N. R., Vitamin B1 Derived Blue and Green Fluorescent Carbon Nanoparticles for Cell-Imaging Application. *ACS Applied Materials & Interfaces* **2014**, 6(10), 7672-7679.
- [60] Nandi, S.; Malishev, R.; Kootery, K. P.; Mirsky, Y.; Kolusheva, S.; Jelinek, R., Membrane Analysis With Amphiphilic Carbon Dots. *Journal Chemical Communications* **2014**, 50(71), 10299-10302.
- [61] Song, Y.; Zhu, S.; Zhang, S.; Fu, Y.; Wang, L.; Zhao, X.; Yang, B., Investigation From Chemical Structure to Photoluminescent Mechanism: A Type of Carbon Dots from The Pyrolysis of Citric Acid and An Amine. *Journal of Materials Chemistry C* **2015**, 3(23), 5976-5984.
- [62] Liu, H.; He, Z.; Jiang, L. P.; Zhu, J. J., Microwave-Assisted Synthesis of Wavelength-Tunable Photoluminescent Carbon Nanodots and Their Potential Applications. *ACS Applied Materials & Interfaces* **2015**, 7(8), 4913-4920.
- [63] Sun, Y. P.; Zhou, B.; Lin, Y.; Wang, W.; Fernando, K. S.; Pathak, P.; Luo, P. G., Quantum-Sized Carbon Dots for Bright and Colorful Photoluminescence. *Journal of the American Chemical Society* **2006**, 128(24), 7756-7757.
- [64] Ali, H.; Bhunia, S. K.; Dalal, C.; Jana, N. R., Red Fluorescent Carbon Nanoparticle-Based Cell Imaging Probe. *ACS Applied Materials & Interfaces* **2016**, 8(14), 9305-9313.
- [65] Jensen, L.; Schatz, G. C., Resonance Raman Scattering of Rhodamine 6G As Calculated Using Time-Dependent Density Functional Theory. *Journal of Physical Chemistry A* **2006**, 110(18), 5973-5977.
- [66] Nie, S.; Emory, S. R., Probing Single Molecules and Single Nanoparticles by Surface-Enhanced Raman Scattering. *Journal of Science* **1997**, 275(5303), 1102-1106.
- [67] Schatz, G. C.; Van Duyne, R. P., Electromagnetic Mechanism of Surface-Enhanced Spectroscopy. *Handbook of Vibrational Spectroscopy* **2002**, 1, 759-774.
- [68] Currie, L. A., Detection: International Update, and Some Emerging Di-Lemmas Involving Calibration, The Blank, and Multiple Detection Decisions. *Journal of Chemometrics and Intelligent Laboratory Systems* 1997, 37(1),151-181.
- [69] Del Río Bocio, F. J.; Riu, J.; Boqué, R.; Rius, F. X., Limits of Detection in Linear Regression With Errors in The Concentration. *Journal of Chemometrics: A Journal of The Chemometrics Society* **2003**, 17(7), 413-421.
- [70] Currie, L. A., Detection and Quantification Limits: Origins and Historical Overview. *Journal of Analytica Chimica Acta* **1999**, 391(2), 127-134.
- [71] Carroll, R. J.; Ruppert, D., The Use and Misuse of Orthogonal Regression in Linear Errors-in-Variables Models. *The American Statistician* **1996**, 50(1), 1-6.
- [72] Miziolek, A. W.; Palleschi, V.; Schechter, I., *Laser induced breakdown spectroscopy*. Cambridge university press. **2006**.
- [73] Araujo, P. Key Aspects of Analytical Method Validation and Linearity Evaluation. *Journal of Chromatography B* **2009**, 877(23), 2224-2234.
- [74] Ribani, M.; Bottoli, C. B. G.; Collins, C. H.; Jardim, I. C. S. F.; Melo, L. F. C., Validation for Chromatographic and Electrophoretic Methods. *Quimica Nova* **2004**, 27(5), 771-780.
- [75] Sesi, N.N.; Hanselman, D. S.; Galley, P.; Horner, J.; Huang, M.; Hieftje, G. M., An Imaging-Based Instrument for Fundamental Plasma Studies. *Journal of Spectrochimica Acta Part B: Atomic Spectroscopy* **1997**, 52(1), 83-102.
- [76] Bokowski, L. V.; SoBRInho, R. B.; Armijo, C. J.; Dani, C.; Henriques, J. A.; Funchal, C., Method Validation for Determination of Metals in Vitis Labrusca L. Grapevine Leaf Extracts by Inductively Coupled Plasma Mass Spectrometry (ICP-MS). *Anais da academia brasileira de ciências* **2016**, 88(4), 2247-2255.

- [77] Santos, M. C.; Nóbrega, J. A., Slurry Nebulization in Plasmas for Analysis of Inorganic Materials. *Journal of Applied Spectroscopy Reviews* **2006**, *41*(4), 427-448.
- [78] Lee, P.; Meisel, D., Adsorption and Surface-Enhanced Raman of Dyes on Silver and Gold Sols. *The Journal of Physical Chemistry* **1982**, *86*(17), 3391-3395.
- [79] Guzmán, M. G.; Dille, J.; Godet, S., Synthesis of Silver Nanoparticles by Chemical Reduction Method and Their Antibacterial Activity. *International Journal of Chemistry Biomolecular Engineering* **2009**, *2*(3), 104-111.
- [80] Amendola, V.; Bakr, O. M.; Stellacci, F., A Study of The Surface Plasmon Resonance of Silver Nanoparticles by The Discrete Dipole Approximation Method: Effect of Shape, Size, Structure, and Assembly. *Journal of Plasmonics* **2010**, *5*(1), 85-97.
- [81] Panda, S. K.; Chakraborti, S.; Basu, R. N., Size and Shape Dependences of The Colloidal Silver Nanoparticles on The Light Sources in Photo-Mediated Citrate Reduction Technique. *Bulletion of Materials Science* **2018**, *41*(4), 90.
- [82] Kanwal, Z.; Raza, M. A.; Riaz, S.; Manzoor, S.; Tayyeb, A.; Sajid I.; Naseem, S., Synthesis and Characterization of Silver Nanoparticle-Decorated Cobalt Nanocomposites (Co@ AgNPs) and Their Density-Dependent Antibacterial Activity. *Journal of Royal Society Open Science* **2019**, *6*(5), 182135.
- [83] Benakashani, F.; Allafchian, A.; Jalali, S., Biosynthesis of Silver Nanoparticles Using *Capparis spinosa* L. Leaf Extract and Their Antibacterial Activity. *Journal of Modern Science* **2016**, *2*(4), 251-258.
- [84] Nain, A.; Barman, S. R.; Jain, S.; Mukherjee, A.; Satija, J., Dual Mechanism-Based Sensing of Mercury Using Unmodified, Heteroepitaxially Synthesized Silver Nanoparticles. *Journal of Applied Nanoscience* **2017**, *7*(6), 299-307.
- [85] Lasio, B.; Malfatti, L.; Innocenzi, P., Photodegradation of Rhodamine 6G Dimers in Silica Sol-Gel Films. *Journal of Photochemistry and Photobiology A: Chemistry* **2013**, *271*, 93-98.
- [86] Schneider, J.; Reckmeier, C. J.; Xiong, Y.; Von Seckendorff, M.; Susha, A. S.; Kasák, P.; Rogach, A. L., Molecular Fluorescence in Citric Acid-Based Carbon Dots. *The Journal of Physical Chemistry C* **2017**, *121*(3), 2014-2022.
- [87] Hoang, Q. B.; Mai, V. T.; Nguyen, D. K.; Truong, D.; Mai, X. D., Crosslinking Induced Photoluminescence Quenching in Polyvinyl Alcohol-Carbon Quantum Dot Composite. *Journal of Materials Today Chemistry* **2019**, *12*, 166-172.
- [88] Sharma, A.; Gady, T.; Neogy, S.; Ghosh, S. K.; Kumbhakar, M., Molecular Origin and Self-Assembly of Fluorescent Carbon Nanodots in Polar Solvents. *The journal of physical chemistry letters* **2017**, *8*(5), 1044-1052.
- [89] Fu, M.; Fu, M.; Ehrat, F.; Wang, Y.; Milowska, K. Z.; Reckmeier, C.; Rogach, A. L.; Feldmann, J., Carbon Dots: A Unique Fluorescent Cocktail of Polycyclic Aromatic Hydrocarbons. *Journal of Nano letters* **2015**, *15*(9), 6030-6035.
- [90] Sastry, M.; Mayya, K.; Bandyopadhyay, K., pH Dependent Changes in The Optical Properties of Carboxylic Acid Derivatized Silver Colloidal Particles. *Colloids and Surfaces A: Physicochemical and Engineering Aspects* **1997**, *127*(1-3), 221-228.
- [91] Gong, Y. J.; Zhang, X. B.; Chen, Z.; Yuan, Y.; Jin, Z.; Mei, L.; Yu, R. Q., An Efficient Rhodamine Thiospirolactam-Based Fluorescent Probe for Detection of Hg²⁺ in Aqueous Samples. *Journal of Analyst* **2012**, *137*(4), 932-938.
- [92] Xia, Y. S.; Zhu, C. Q., Use of Surface-Modified CdTe Quantum Dots as Fluorescent Probes in Sensing Mercury (II). *Journal of Talanta* **2008**, *75*(1), 215-221.
- [93] Bhunia, S. K.; Maity, A. R.; Nandi, S.; Stepensky, D.; Jelinek, R., Imaging Cancer Cells Expressing The Folate Receptor With Carbon Dots Produced From Folic Acid. *Journal of ChemBioChem* **2016**, *17*(7), 614-619.
- [94] Baker, S. N.; Baker, G. A., Luminescent Carbon Nanodots: Emergent Nanolights. *Angewandte Chemie International Edition* **2010**, *49*(38), 6726-6744.
- [95] Bhunia, S. K.; Saha, A.; Maity, A. R.; Ray, S. C.; Jana, N. R., Carbon Nanoparticle-

- Based Fluorescent Bioimaging Probes. *Journal of Scientific reports* **2013**, 3(1), 1-7.
- [96] Vinogradova, E.; Tlahuice-Flores, A.; Velazquez-Salazar, J. J.; Larios-Rodriguez, E.; Jose-Yacaman, M., Surface-Enhanced Raman Scattering of N-Acetylneuraminic Acid on Silver Nanoparticle Surface. *Journal of Raman Spectroscopy* **2014**, 45(9), 730-735.
- [97] Binkley, J. S.; Pople, J. A.; Hehre, W. J., Self-Consistent Molecular Orbital Methods. 21. Small Split-Valence Basis Sets for First-Row Elements. *Journal of the American Chemical Society* **1980**, 102(3), 939-947.
- [98] Nasdala, L.; Smith, D. C.; Kaindl, R.; Ziemann, M. A., Raman Spectroscopy: Analytical Perspectives in Mineralogical Research. *Journal of Spectroscopic methods in mineralogy* **2004**, 6, 281-343.
- [99] Dutta, S.; Sarkar, S.; Ray, C.; Roy, A.; Sahoo, R.; Pal, T., Mesoporous Gold and Palladium Nanoleaves From Liquid–Liquid Interface: Enhanced Catalytic Activity of The Palladium Analogue Toward Hydrazine-Assisted Room-Temperature 4-Nitrophenol Reduction. *ACS applied materials & interfaces* **2014**, 6(12), 9134-9143.
- [100] Klingsporn, J. M.; Jiang, N.; Pozzi, E. A.; Sonntag, M. D.; Chulhai, D.; Seideman, T.; Duyne, R. P. V., Intramolecular Insight Into Adsorbate–Substrate Interactions via Low-Temperature, Ultrahigh-Vacuum Tip-Enhanced Raman Spectroscopy. *Journal of the American Chemical Society* **2014**, 136(10), 3881-3887.
- [101] Deng, H.; Yu, H., Self-Assembly of Rhodamine 6G on Silver Nanoparticles. *Journal of Chemical Physics Letters* 2018, , 692, 75-80.
- [102] Chai, F.; Wang, C.; Wang, T.; Ma, Z.; Su, Z., L-Cysteine Functionalized Gold Nanoparticles For The Colorimetric Detection of Hg²⁺ Induced by Ultraviolet Light. *Journal of Nanotechnology* **2009**, 21(2), 025501.

VITA

NAME	Andaru Dena Prasiwi
DATE OF BIRTH	27 March 1995
PLACE OF BIRTH	Banyumas, Central Java, Indonesia
INSTITUTIONS ATTENDED	Chulalongkorn University, Thailand.
HOME ADDRESS	SK Apartment Charoenpol, 577/3 Banthatong Rd, Wangmai, Pathumwan, Bangkok 10330.
PUBLICATION	Proceeding of "Surface-Enhanced Raman Scattering using Fluorescence-Quenched Carbon Quantum Dots for Mercury Ion Detection" pp. 520-528. The 46th International Congress on Science, Technology and Technology-based Innovation 2020 (October 5-7, 2020)